NASA Contractor Report 178231

ICASE REPORT NO. 87-2

ICASE

EVOLUTION OF A LOCALIZED THERMAL EXPLOSION IN A REACTIVE GAS

T. L. Jackson

A. K. Kapila

D. S. Stewart

Contract No. NAS1-18107

January 1987

INSTITUTE FOR COMPUTER APPLICATIONS IN SCIENCE AND ENGINEERING
NASA Langley Research Center, Hampton, Virginia 23665

Operated by the Universities Space Research Association

National Aeronautics and
Space Administration

Langley Research Center
Hampton, Virginia 23665

EVOLUTION OF A LOCALIZED THERMAL EXPLOSION IN A REACTIVE GAS

T. L. Jackson*, A. K. Kapila# and D. S. Stewart**

Abstract

Experimental observations of ignition in premixed gaseous reactants indicate that perfectly homogeneous initiation is practically unrealizable. Instead, combustion first sets in, as a rule, at small, discrete sites where inherent inhomogeneities cause chemical activity to proceed preferentially and lead to localized explosions. Combustion waves propagating away from these "hot spots" or "reaction centers" eventually envelope the remaining bulk.

This study examines the spatial structure and temporal evolution of a hot spot for a model involving Arrhenius kinetics. The hot spot, characterized by peaks in pressure and temperature with little diminution in local density, is shown to have one of two possible self-similar structures. The analysis employs a combination of asymptotics and numerics, and terminates when pressure and temperature in the explosion have peaked.

* Institute for Computer Applications in Science and Engineering
NASA Langley Research Center, Hampton, Virginia 23665
and
Department of Mathematical Sciences
Old Dominion University, Norfolk, Virginia 23508

Department of Mathematical Sciences
Rensselaer Polytechnic Institute, Troy, New York 12180-3590

** Department of Theoretical and Applied Mechanics
University of Illinois, Urbana, Illinois 61801

This work was supported by the U.S. Army Research Office, by the National Aeronautics and Space Administration under NASA Contract NAS1-18107, and by the the Los Alamos National Laboratories.

1. Introduction

This paper descibes mathematically the birth and growth of a hot spot, or localized thermal explosion, in a premixed reactive gas.

Experimental observations on the initiation of combustion in gases at high temperatures, in shock tubes and elsewhere, have demonstrated conclusively that spatially homogeneous combustion is essentially an unattainable ideal. In fact, ignition first sets in locally, in small volume elements at discrete sites, where chemical reaction proceeds preferentially due to inherent imperfections in the system. In due course, combustion waves originating from localized explosions occuring at these "hot spots", "reaction centers" or "exothermic centers" envelope the entire reacting mass. The role played by these sites as precursors of more dramatic combustion phenomena is revealed with unsurpassed clarity in Urtiew and Oppenheim's [1] photographic records of deflagration-to-detonation transition in a Hydrogen-Oxygen mixture confined to a tube. These photographs show that as the deflagration travels down the tube, it accelerates and evolves into a highly folded turbulent flame, preceded by a so-called precursor shock. Eventually, an exothermic center is formed in the vicinity of the flame, near the tube wall. The localized explosion in this center creates a blast wave which propagates through the preconditioned mixture behind the precursor shock and ultimately evolves into a fully-developed detonation. The same feature appears in other modes of detonation-initiation, as well as in other geometric configurations.

The early analyses of reaction-center dynamics are due to Zajac and Oppenheim [2] and Meyer and Oppenheim [3]. In these studies

the reaction center is assumed to be a spatially homogeneous source of chemical energy, capable of expansion and separated from its inert surroundings by an impermeable barrier, across which only momentum transfer can occur. Either by prescribing a specific reaction scheme, or by specifying an energy release profile within the center, the above authors were able to compute the resulting pressure pulse.

In this paper the reaction center is treated as part and parcel of the reacting medium rather than an isolated entity in an inert atmosphere, and is found to have a definite spatial structure. The aim of this paper is to describe this structure and to study its temporal evolution in a plane, one-dimensional framework, under the asssumption that the reactive gas undergoes a single, one-step, first-order, irreversible chemical reaction of the Arrhenius type. One may argue that the simple overall kinetic scheme adopted here is too idealized to be realistic. However, for large activation energies, the kinetics does capture an essential attribute of most combustion systems, namely, a reaction rate which accelerates rapidly with increase in temperature. Thus the model is quite appropriate for studying problems, such as the one at hand, which owe their genesis to the interaction between gasdynamics and chemical heat release at highly temperature-sensitive rates.

The configuration of the system is so prescribed as to provoke the development of a single hot spot, and this can be accomplished in a variety of ways. For example, the shock-induced thermal-runaway studies of Clarke and Cant [4] and Jackson and Kapila [5]

considered a semi-infinite expanse of gas ignited by a piston-driven shock, thereby creating a hot spot at the piston face. Instead, the present work assumes that the gas is confined between two parallel planes, and that its initial state possesses a slight spatial nonuniformity. (In a practical situation these non-uniformities may be caused by a variety of factors, such as turbulence, interacting pressure waves, or, in the case of condensed explosives, material imperfections.) The mathematical model leads to an initial-boundary value problem for the equations of reactive gasdynamics. An asymptotic solution is developed in the limit of large activation energy, and the analysis is carried as far as the end of the localized explosion within the center. The subsequent expansion of the center, and the eventual generation of a blast wave, will be the subject of a future publication.

The temporal evolution of the explosion occurs in two stages, beginning with the induction stage. Here the state of the gas is a small perturbation of the initial state and the underlying physical processes are those of linearized acoustics coupled to a weak but nonlinear chemical reaction. The reduced equations require a numerical solution (see [4] and [5]) which exhibits local thermal runaway. Induction is followed by the explosion stage, which consists of several distinct spatial zones. There is the practically frozen **outer zone**, and a rapidly shrinking **inner zone** or **layer** in which intense chemical activity leads to an explosive growth of temperature and pressure. Nonlinear chemistry is again coupled to linearized gasdynamics, but now the linearization is about an atmosphere undergoing a spatially homogeneous thermal

explosion. As the layer shrinks, it recedes away from the outer zone, thereby creating an **intermediate zone** which is frozen in time. Although highly nonlinear, the explosion stage is amenable to analysis because gasdynamics is of secondary importance; temporal variations are much too rapid for the gas to undergo significant expansion.

For the specific reaction scheme under consideration it is found that the reaction center can have one of two posible spatial structures, depending upon whether the temperature profile within the hot spot has a sharp peak or a rounded peak (Figure 1). The former typifies hot spots originating at boundaries (e.g., a piston face), and the latter those occuring in the interior of the vessel. These structures, which will be referred to as the **"Type B"** (boundary-type) or **"Type I"** (internal type), are both self-similar. The former is described below in detail, with only the results for the latter given in section 6. In addition to these two structures there exists a third, described briefly in the Appendix; it is singular and corresponds to very special initial conditions.

The specific configuration under study here was also examined, with similar methods, by Poland and Kassoy [6]. Their analysis differs from ours in one crucial respect; they considered the distinguished limit in which the spatially homogeneous induction time at the initial state and the conduction time across the vessel are of the same order, i.e., the Frank-Kamanetskii number δ is of order unity, albeit supercritical. In our analysis the induction time is comparable to the **acoustic** time across the vessel, i.e., δ is very large. In physical terms, the explosive mixture being

considered here has a faster reaction rate.

2. The Basic Equations, and Setup

The equations of reactive gasdynamics for plane, one-dimensional, unsteady motion are [7]

$$\rho_t + u\rho_x + \rho u_x = 0, \tag{2.1a}$$

$$\rho(u_t + uu_x) + (1/\gamma)p_x = 0, \tag{2.1b}$$

$$\rho(T_t + uT_x) - [(\gamma-1)/\gamma](p_t + up_x) = \beta w, \tag{2.1c}$$

$$\rho(Y_t + uY_x) = -w, \tag{2.1d}$$

$$p = \rho T, \tag{2.1e}$$

where

$$w = [1/(\beta\theta)]\rho Y\exp(\theta-\theta/T). \tag{2.1f}$$

Here p, ρ, T, u and Y are, respectively, the gas pressure, density, temperature, velocity and reactant mass fraction. The variables have been made dimensionless with respect to a constant reference state p_0, ρ_0, T_0 and Y_0. Velocity is referred to the acoustic speed c_0, defined by

$$c_0 = [\gamma p_0/\rho_0]^{1/2},$$

time to t_0, the homogeneous induction time at the reference state, and length to c_0t_0. The diffusion terms have been left out because they are much too small to play a role in the problem under study.

The dimensionless parameters appearing above are the specific-heats ratio γ, the chemical heat release β and the activation energy θ.

Let the reacting gas be confined to the interval $0 < x < a$. At the walls the appropriate boundary conditions are

$$(2.2) \qquad u(0,t) = u(a,t) = 0.$$

The initial state of the gas is taken to be an $O(\theta^{-1})$ perturbation of the spatially homogeneous and stationary reference state, i.e.,

$$(2.3a) \qquad u(x,0) = \theta^{-1}u_1(x,0),$$

$$(2.3b) \qquad \Phi(x,0) = 1 + \theta^{-1}\Phi_1(x,0) \text{ for } \Phi = T,\ p,\ Y \text{ and } \rho,$$

where the precise specification of $u_1(x,0)$ and $\Phi_1(x,0)$ must await the next section. Note that

$$(2.3c) \qquad \rho_1(x,0) = p_1(x,0) - T_1(x,0)$$

in accordance with the gas law (2.1e). An asymptotic solution of the initial-boundary-value problem (2.1)-(2.3) is sought in the limit $\theta \to \infty$, with β and γ fixed and $O(1)$, until the localized explosion has reached completion. The various stages of evolution are detailed in the following sections.

3. The Induction Stage

The initial conditions (2.3) suggest that, at least initially, the state of the gas remains an $O(\theta^{-1})$ perturbation of the

reference state. During this period, referred to as the induction stage, one therefore seeks the expansions

$$(3.1) \qquad u \sim \theta^{\frac{1}{4}} u_1 + \ldots, \quad \Phi \sim 1 + \theta^{-1}\Phi_1 + \ldots, \qquad \text{for } \Phi = T,\ p,\ Y \text{ and } \rho$$

which, upon substitution into the set (2.1) yield the leading-order disturbance equations

$$(3.2a) \qquad (\partial/\partial t \pm \partial/\partial x)(p_1 \pm \gamma u_1) = \gamma \exp(T_1),$$

$$(3.2b) \qquad \partial/\partial t[\gamma T_1 - (\gamma-1)p_1] = \gamma \exp(T_1),$$

$$(3.2c) \qquad \rho_1 = p_1 - T_1, \quad \partial Y_1/\partial t = -(1/\beta)\exp(T_1).$$

Except for the nonlinear source term, eqns. (3.2a,b) are simply those of linearized acoustics in a uniform atmosphere. It is a simple matter to integrate them along the characteristics, as was done in [4] and [5] for a different configuration. During induction it is enough to concentrate on the variables T_1, p_1 and u_1, because once they are known, the first eqn. in (3.2c) yields ρ_1 while the second, combined with (3.2b) and integrated, determines Y_1 according to the expression

$$(3.2d) \qquad T_1 - [(\gamma-1)/\gamma]p_1 + \beta Y_1 = T_1(x,0) - [(\gamma-1)/\gamma]p_1(x,0) + \beta Y_1(x,0).$$

Equations (3.2) need to be solved numerically, and this was done for

$\gamma = 1.4$

and for a variety of smooth initial conditions and interval lengths a. A high-resolution, adaptive ODE integrator was employed to integrate along the characteristics. All computations displayed thermal runaway, characterized by the unboundedness of T_1 and p_1 somewhere in the interval [0,a] at a finite time t_e. The numerical results can all be summarized by considering two representative cases, for which the initial values of pressure and mass fraction correspond to those at the reference state and the initial velocity is zero, i.e.,

(3.3a) $$p_1(x,0) = Y_1(x,0) = u_1(x,0) = 0,$$

while the initial temperature perturbations are prescribed as

(3.3b) $T_1(x,0) = b[1-(x/a)]$ for case I, $b[1-(x/a)^2]$ for case II.

(Numerical results to be presented below correspond to a = 0.8, b = 0.5.) In both cases the initial disturbance has a single maximum at x = 0, causing it to become the site of thermal runaway. The essential difference between the two cases is that in I the temperature disturbance has a nonzero spatial gradient (sharp peak) and in II a zero spatial gradient (rounded peak), at x = 0. Thus I typifies a hot spot located at the boundary (e.g., the shock configuration discussed in [4] and [5]), and II an internal hot spot (easily visualized by a symmetric reflection about the

origin). Henceforth the two cases will be referred to, respectively, as Type B (boundary) and Type I (internal). Their spatial structures, it turns out, are different.

In the following sections the Type-B problem is discussed in detail. The Type-I problem can be treated analogously and is, in fact, slightly simpler to analyze; it was deemed sufficient, therefore, to simply state its solution in section 6.

We start with Figure 2, which displays the numerical results for the Type-B induction solution. The four graphs there exhibit, respectively, the profiles of T_1, p_1, u_1 and ρ_1 against x for increasing values of t, upto the time beyond which the integration routine was unsuccessful for a time step 10^{-6}, thus signalling the imminence of blowup. An examination of the T_1- profile near blowup reveals the birth of a boundary layer at x = 0. Additional information is provided by Figure 3, where the function $\exp[-T_1(0,t)]$ is graphed near blowup. The straight-line graph in the figure has slope 1.4 (=γ), and a t-intercept equal to the blowup time t_e, allowing one to conclude that

$$T_1(0,t) \sim -\ell n[\gamma(t_e-t)] + o(1) \text{ as } t \to t_e. \tag{3.4}$$

Figure 4 displays time plots of the solution at x = 0, and shows clearly that while $T_1(0,t)$ and $p_1(0,t)$ become unbounded, $\rho_1(0,t)$ does not. Therefore, $p_1(0,t)$ must have precisely the same leading-order behavior as $T_1(0,t)$, i.e.,

$$p_1(0,t) \sim -\ell n[t_e-t] + O(1) \text{ as } t \to t_e. \tag{3.5}$$

To summarize, the induction stage exhibits the classic logarithmic singularity of spatially homogeneous thermal runaway [8].

4. Type-B Blowup Structure

Although numerics has elucidated the temporal character of the blowup singularity, further analysis is needed to ascertain its spatial structure. This will be done by examining separately the boundary layer, whose emergence has already been noted, and the region outside. First, it is convenient to introduce a new time variable τ via the expression

$$\tau = t_e - t, \quad \tau > 0. \tag{4.1}$$

Then, following simple manipulations, eqns. (3.2a,b) transform into

$$\partial p_1/\partial x - \gamma \partial u_1/\partial \tau = 0, \tag{4.2a}$$

$$\gamma \partial u_1/\partial x - \partial p_1/\partial \tau = (\gamma-1)\partial p_1/\partial \tau - \gamma \partial T_1/\partial \tau = \gamma \exp(T_1), \tag{4.2b}$$

where the dependent variables are now treated as functions of x and τ. The relevant boundary condition is the first of (2.2), re-written as

$$u_1(0,\tau) = 0. \tag{4.3}$$

Elementary manipulations on (4.2a,b) and (4.3) yield the following integral, which will prove to be of value later on:

$$(4.4) \qquad \mathcal{J}(\tau) = \mathcal{J}_0 \exp\Big[\int_{\tau}^{t_e} \exp(T_1(0,t))dt\Big],$$

where $\mathcal{J}(\tau)$ denotes the disturbance temperature gradient at $x = 0$, and $\mathcal{J}_0$ its initial value, i.e.,

$$(4.5) \qquad \mathcal{J}(\tau) = \big[\partial T_1(x,\tau)/\partial x\big]_{x=0}, \quad \mathcal{J}_0 = \mathcal{J}(t_e-).$$

Recall, from (3.3b), that $\mathcal{J}_0$ vanishes for type I but is negative for type B. Then (4.4) shows that $\mathcal{J}(\tau) \equiv 0$ (rounded peak) for the former and decreases monotonocally to $-\infty$ (sharp peak approaching a cusp) for the latter as $\tau \to 0+$.

4.1 The Boundary Layer

Turning now to the asymptotic analysis near blowup, eqns. (4.2a,b) govern the region outside the boundary layer, where the outer limit process

$$x > 0 \text{ and fixed}, \quad \tau \to 0$$

applies. The boundary layer, on the other hand, corresponds to the inner limit process

$$s > 0 \text{ and fixed}, \quad \tau \to 0,$$

where $s(x,\tau)$ is the spatial coordinate in the boundary layer, reflecting its self-similar structure. The shrinking nature of the layer requires x to vanish under the inner limiting process, and

then a moment's reflection suggests the definition

$$(4.6) \qquad s = x/\tau,$$

which assigns coequal importance to the x- and τ-derivatives, thereby providing the richest equations for the inner limit. (It will transpire that this scaling does not quite cover the entire boundary layer, but more about that later.) These equations, obtained by transforming (4.2a,b) to the (s,τ) variables, are

$$(4.7a) \qquad (s\partial/\partial s - \tau\partial/\partial\tau)[\gamma T_1 - (\gamma-1)p_1] = \gamma\tau\exp(T_1),$$

$$(4.7b) \qquad (s\partial/\partial s - \tau\partial/\partial\tau)p_1 + \gamma\partial u_1/\partial s = \gamma\tau\exp(T_1),$$

$$(4.7c) \qquad (s\partial/\partial s - \tau\partial/\partial\tau)u_1 + (1/\gamma)\partial p_1/\partial s = 0.$$

It is convenient to isolate the temporal singularity from the spatial structure, by setting

$$(4.8a) \qquad T_1 = -\ell n(\gamma\tau) + f(s,\tau),$$

$$(4.8b) \qquad p_1 = -\ell n(B_1\tau) + g(s,\tau),$$

$$(4.8c) \qquad u_1 = h(s,\tau),$$

where the yet unknown constant B_1 represents a weak influence of the initial conditions on the self-similar boundary layer, and will be determined in due course by matching. The structure functions f, g and h are assumed to be $o(1)$ in the limit $\tau \to 0$. Substitution of (4.8) into (4.7) yields the structure equations

(4.9a) $$sf_s - \tau f_\tau + (\gamma-1)h_s = e^f - 1,$$

(4.9b) $$s(f_s - g_s) - \tau(f_\tau - g_\tau) - h_s = 0,$$

(4.9c) $$sh_s - \tau h_\tau + (1/\gamma)g_s = 0.$$

The only boundary condition appropriate for the above set is the wall condition

(4.10) $$h(0,\tau) = 0.$$

In addition, since the initial data are smooth, the structure functions and their s-derivatives are required to be regular in s. Consider the asymptotic expansions

(4.11) $$\Phi \sim \sigma_1(\tau)\Phi_1(s) + \sigma_2(\tau)\Phi_2(s) + \ldots \text{ for } \Phi = f, g, \text{ and } h,$$

as $\tau \to 0$. The gauge sequence $\{\sigma_n(\tau)\}$ is not yet specified, but a clue as to its identity is provided by the integral relation (4.4), rewritten as

(4.12) $$f_s(0,\tau) = \mathcal{J}_0\, \tau \exp\left[-\int_{t_e}^{\tau} (1/(\gamma t)\exp\{f(0,t)\}dt\right]$$

in view of the scaling (4.6) and the prescription (4.8). For small τ the f-expansion in (4.11) allows the above relation to be reduced further to the asymptotic form

(4.13) $$\sigma_1 f_1'(0) + \ldots = \mathcal{J}_0 \tau^{\lambda} \exp\left[O(1) - \{f_1(0)/\gamma\}\int_0^{\tau} t^{-1}\sigma_1(t)\, dt + \ldots\right],$$

where

(4.14) $\lambda = (\gamma-1)/\gamma.$

Recall, from (4.5), that the constant $\mathcal{J}_0$ is nonzero for the Type-B problem. Then, the assumption that $f_1'(0)$ is nonvanishing (involving no loss of generality) leads to the conclusion

(4.15) $\sigma_1(\tau) = \tau^{\lambda}$

if the two sides of (4.13) are to balance at leading order. With σ_1 determined, it can be shown that the expansions (4.11) proceed in powers of τ^{λ}.

The boundary-layer analysis can now be carried out, and as hinted earlier, the layer is found to have a two-sublayer structure. It is convenient to refer to Figure 5 in which the various spatial regimes near and beyond blowup are displayed schematically. OR refers to the outer region and BL to the boundary layer; the latter is subdivided further into an interior sublayer L_I and an exterior sublayer L_E. We shall first examine the interior sublayer, show that it becomes nonuniform for large s, determine the appropriate scaling and expansions for the exterior sublayer, and demonstrate that the latter merges smoothly into the outer region. Only one or two terms of the expansions in each region will be computed; continuation to higher orders is straightforward though increasingly complex algebraically.

4.1.1 The Interior Sublayer L_I

Substitution of (4.11) into (4.9) yields the leading-order

structure equations for the inner sublayer,

$$(4.16a) \qquad sf_1' - (\lambda+1)f_1 + (\gamma-1)h_1' = 0,$$

$$(4.16b) \qquad s(f_1'-g_1') - \lambda(f_1-g_1) - h_1' = 0,$$

$$(4.16c) \qquad sh_1' - \lambda h_1 + (1/\gamma)g_1' = 0.$$

The boundary condition

$$(4.16d) \qquad h_1(0) = 0$$

comes from (4.10), and the solution is restricted additionally by the requirement that it be regular. If g_1 and h_1 are eliminated from (4.16a-c), the result is the third-order equation

$$(4.17) \qquad [(s^3-s)f_1']'' + \lambda[(1-3s^2)f_1']' - (s^2-1/\gamma)f_1'' + (\lambda+1)(3\lambda-4)sf_1' + (\lambda^2-1)(2-\lambda)f_1 = 0$$

for f_1. The points s=0 and s=1 are singular points of this equation and the three linearly independent solutions have the asymptotic behavior

$$1,\ s \text{ and } s\ell ns \text{ as } s \to 0, \text{ and}$$

$$1,\ 1-s \text{ and } |1-s|^{3(\gamma-1)/2\gamma} \text{ as } s \to 1.$$

In general one can expect a one-parameter family of regular solutions to exist, and numerical computations verify that such is indeed the case. A convenient parameter is

(4.18) $A_1 \equiv f_1(0)$.

With f_1 known, h_1' can be eliminated from (4.16a,b) to obtain a first-order differential equation for g_1 whose regular solution turns out to be

$$(4.19a) \qquad g_1 = [(\gamma+1/\lambda)/(\gamma-1)]f_1 - [s^\lambda/\lambda(\gamma-1)]\int_0^\tau x^{-\lambda} f_1'(x)dx,$$

and then, (4.16c) integrates to give

$$(4.19b) \qquad h_1 = g_1'/(\gamma\lambda) - [s^\lambda/(\gamma\lambda)]\int_0^\tau x^{-\lambda} g_1''(x)dx,$$

where regularity has been imposed again. Thus the full solution at this order depends on the single parameter A_1. Graphs of f_1, g_1 and h_1 for $A_1 = 1$ are drawn in Figure 6.

At this stage the solution (4.8) has the following expansions in the interior sublayer:

$$(4.20a) \qquad T_1 \sim -\ell n(\gamma\tau) + \tau^\lambda f_1(s) + \ldots,$$

$$(4.20b) \qquad p_1 \sim -\ell n(B_1\tau) + \tau^\lambda g_1(s) + \ldots,$$

$$(4.20c) \qquad u_1 \sim \tau^\lambda h_1(s) + \ldots .$$

In order to determine the spatial extent of L_I one needs the asymptotic behavior of f_1, g_1 and h_1 for large s. This is easily obtained from (4.17) and (4.19), as

$$(4.21a) \qquad f_1 \sim -A_1\alpha[s^{(2\gamma-1)/\gamma} + s^{-1/\gamma}(A_f \ell ns + B_f)$$

$$+ C_f s^{-(\gamma+1)/\gamma} + \ldots],$$

(4.21b) $$g_1 \sim -A_1\alpha[s^{(2\gamma-1)/\gamma} + D_g s^{(\gamma-1)/\gamma} + s^{-1/\gamma}(A_g \ell n s + B_g) + C_g s^{-(\gamma+1)/\gamma} + \ldots],$$

(4.21c) $$h_1 \sim -A_1\alpha[s^{(\gamma-1)/\gamma}(A_h \ell n s + B_h) + C_h s^{-1/\gamma} + \ldots].$$

Here α, B_f and C_f are constants with values

$$\alpha = 2.660, \quad B_f = -0.236, \quad C_f = 0.0737$$

obtained by integrating the f_1 equation (4.17) numerically. The remaining constants appearing above are given by

$$A_f = -(2\gamma-1)(\gamma-1)^2/(2\gamma^3), \quad A_g = (\gamma+1)A_f/(\gamma-1),$$
$$A_h = 2A_f\gamma/(\gamma-1)^2, \quad B_g = A_f/(\gamma-1) + (\gamma+1)B_f/(\gamma-1),$$
(4.22) $$B_h = 2B_f\gamma/(\gamma-1)^2 - \gamma(3\gamma-1)A_f/(\gamma-1)^3,$$
$$C_g = (2\gamma+1)C_f/(2\gamma-2), \quad C_h = -3\gamma C_f/(\gamma-1),$$
$$D_g = -3C_f\gamma^3/(\gamma-1)^2.$$

The range of validity of the expansions (4.20) can now be determined. For example, substitution of (4.21a) into (4.20a) suggests that the latter becomes nonuniform when

$$\tau^{\lambda} s^{(2\gamma-1)/\gamma} = O(1), \text{ i.e., } s = O(\tau^{-\mu}),$$

where

(4.23) $$\mu = (\gamma-1)/(2\gamma-1)$$

and the definition (4.14) of λ has been invoked. Correspondingly,

$$x = O(\tau^{\gamma/(2\gamma-1)}) = o(1).$$

The smallness of x indicates that although one has reached the edge of L_I, the outer region is still too far. The need for an exterior sublayer is therefore apparent.

4.1.2 The Exterior Sublayer L_E

In this sublayer the appropriate variables are ξ and τ, with ξ defined by

$$\xi = \tau^{\mu} s \equiv x/\tau^{\gamma/(2\gamma-1)}. \tag{4.24}$$

The expressions (4.8) for T_1, p_1 and u_1 hold again, provided f, g and h are now treated as functions of ξ and τ. The structure equations, obtained from (4.9) by transforming from s to ξ, are

$$(1-\mu)\xi f_{\xi} - \tau f_{\tau} + (\gamma-1)\tau^{\mu} h_{\xi} = e^{f}-1, \tag{4.25a}$$

$$(1-\mu)\xi(f_{\xi}-g_{\xi}) - \tau(f_{\tau}-g_{\tau}) - \tau^{\mu} h_{\xi} = 0, \tag{4.25b}$$

$$(1-\mu)\xi h_{\xi} - \tau h_{\tau} + (1/\gamma)\tau^{\mu} g_{\xi} = 0. \tag{4.25c}$$

Matching requirements imposed by L_I, obtained by substituting (4.21) into (4.20) and then employing (4.24), are

$$f \sim -A_1\alpha\, \xi^{(2\gamma-1)/\gamma} + O(\tau^{2\mu}\, \ell n\tau), \tag{4.26a}$$

$$g \sim -A_1\alpha\, \xi^{(2\gamma-1)/\gamma} + O(\tau^{\mu}), \tag{4.26b}$$

(4.26c) $$h \sim -A_1\alpha\,\tau^{\mu}\,\xi^{(\gamma-1)/\gamma}[A_h(-\mu\,\ell n\tau + \ell n\xi) + B_h] + O(\tau^{2\mu}),\ \text{as}\ \xi \to 0.$$

Guided by these the L_E solution is sought in the form

(4.27a) $$f \sim F_0(\xi) + \ldots,$$

(4.27b) $$g \sim G_0(\xi) + \ldots,$$

(4.27c) $$h \sim \tau^{\mu}[\ell n\tau\, H_0(\xi) + H_1(\xi)] + \ldots .$$

Substitution into (4.25) leads to the differential equations

$$(1-\mu)\xi F_0' = \exp(F_0)-1,$$

$$F_0' - G_0' = 0,$$

$$(1-\mu)\xi H_0' - \mu H_0 = 0,$$

$$(1-\mu)\xi H_1' - \mu H_1 = H_0 - (1/\gamma)G_0',$$

whose solutions, subject to the matching requirements (4.26), are

(4.28a) $$F_0(\xi) = G_0(\xi) = -\ell n[1+A_1\alpha\xi^{(2\gamma-1)/\gamma}],$$

(4.28b) $$H_0(\xi) = -A_1\alpha\{(\gamma-1)/\gamma^2\}\xi^{(\gamma-1)/\gamma},$$

(4.28c) $$H_1(\xi) = A_1\alpha\,\xi^{(\gamma-1)/\gamma}[\{(2\gamma-1)/\gamma^2\}\{\ell n\xi + F_0(\xi)\} - B_h].$$

Thus the L_E-solution can be written as

(4.29a) $$T_1 \sim -\ell n(\gamma\tau) + F_0(\xi) + \ldots,$$

(4.29b) $$p_1 \sim -\ell n(B_1\tau) + F_0(\xi) + \ldots,$$

(4.29c) $$u_1 \sim \tau^{\mu}\,[\ell n\tau\, H_0(\xi) + H_1(\xi)] + \ldots .$$

One must consider the behavior of this solution for large ξ in order to assess the spatial extent of the sublayer L_E. This can be done, for example, by substituting the large-ξ behavior of (4.28a) into (4.29a). The result is the expansion

$$T_1 \sim -\{(2\gamma-1)/\gamma\}\ell n(\tau^{\gamma/(2\gamma-1)}\xi) - \ell n(A_1\alpha\gamma) + \ldots,$$
$$\text{as } \xi \to \infty,$$

which clearly becomes disordered when $\xi = O(\tau^{-\gamma/(2\gamma-1)})$. Correspondingly, $x = O(1)$, indicating that the edge of the boundary layer has now been reached. The next step is to see if the boundary layer merges smoothly with the region OR.

4.2 The Outer Region OR

In the outer region, where x and τ are the proper variables, the solution can be expanded as

(4.30) $$\Phi_1 \sim \Phi_{10}(x,t_e) + \tau\,\Phi_{11}(x) + \ldots, \text{ for } \Phi_1 = T_1,\ p_1 \text{ and } u_1,$$

where the leading terms are the numerically obtained limiting values at blowup and the higher-order terms can be computed from (4.2a,b) under the outer limit process. It is a straightforward matter to establish that a match of (4.30) with the L_E-solution (4.29a-c) requires the following asymptotic behavior of the outer solution at blowup:

(4.31a) $$T_1 \sim -\{(2\gamma-1)/\gamma\}\ell nx - \ell n(A_1\alpha\gamma) + \ldots,$$

(4.31b) $$p_1 \sim -\{(2\gamma-1)/\gamma\}\ell n x - \ell n(A_1\alpha B_1) + \ldots,$$

(4.31c) $$u_1 \sim -A_1\alpha\, x^{(\gamma-1/\gamma)}\left[\{(2\gamma-1)/\gamma^2\}[\{(\gamma-1)/\gamma\}\ell n x + \ell n(A_1\alpha)]+B_h\right] + \ldots, \text{ as } x \to 0.$$

A careful examination of the numerical solution does, indeed, confirm this behavior. The constants A_1 and B_1, the only ones yet undetermined, can then be found by comparing the above expansions with the numerical solution. The comparison is made at the "edge" of the boundary layer, i.e., for (x,τ) satisfying $\tau \ll 1$, $\tau^{\gamma/(2\gamma-1)} \ll x \ll 1$. It should be emphasized that the structure of the blowup singularity is influenced by the initial conditions only via these constants; otherwise, the solution has a universal, self-similar structure.

4.3 Summary

The near-blowup analysis is now complete, and can be summarized. In the interior sublayer L_I the expansions are

(4.32a) $$T \sim 1 + \theta^{-1}[-\ell n(\gamma\tau) + \tau^{\lambda} f_1(s) + \ldots] + \ldots,$$

(4.32b) $$p \sim 1 + \theta^{-1}[-\ell n(B_1\tau) + \tau^{\lambda} g_1(s) + \ldots] + \ldots,$$

(4.32c) $$u \sim \theta^{-1}[\tau^{\lambda} h_1(s) + \ldots] + \ldots,$$

where f_1, g_1 and h_1 are defined by (4.17) and (4.19). In the exterior sublayer, the solution is

(4.33a) $$T \sim 1 + \theta^{-1}[-\ell n(\gamma\tau) + F_0(\xi) + \ldots] + \ldots,$$

(4.33b) $$p \sim 1 + \theta^{-1}[-\ell n(B_1\tau) + F_0(\xi) + \ldots] + \ldots,$$

(4.33c) $\quad u \sim \theta^{-1}[\tau^{\mu}\, \ell n\tau\, H_0(\xi) + \tau^{\mu}\, H_1(\xi) + \ldots] + \ldots,$

where F_0, H_0 and H_1 are given by (4.28). In the outer region the expansions take the form

(4.34a) $\quad T \sim 1 + \theta^{-1}[T_{10}(x,t_e) + O(\tau)] + \ldots,$

(4.34b) $\quad p \sim 1 + \theta^{-1}[p_{10}(x,t_e) + O(\tau)] + \ldots,$

(4.34c) $\quad u \sim \theta^{-1}[u_{10}(x,t_e) + O(\tau)] + \ldots,$

where T_{10}, p_{10} and u_{10} are the terminal values of the induction solution, determined numerically.

The remaining variables ρ and Y can be computed, upto $O(\theta^{-1})$, by appealing to the first equation of (3.2c) and (3.2d). The results are

(4.35a) $\quad \rho \sim 1 + \theta^{-1}[\ell n(\gamma/B_1) + \tau^{\lambda}\,(g_1-f_1) + \ldots] + \ldots,$

(4.35b) $\quad Y \sim 1 + (\theta\beta\gamma)^{-1}[\ell n(b_1\tau) + \tau^{\lambda}\,\{(\gamma-1)g_1-\gamma f_1\} + \ldots] + \ldots$

in L_I,

(4.36a) $\quad \rho \sim 1 + \theta^{-1}[\ell n(\gamma/B_1) + \ldots] + \ldots,$

(4.36b) $\quad Y \sim 1 + (\theta\beta\gamma)^{-1}[\ell n(b_1\tau) - F_0(\xi) + \ldots] + \ldots$

in L_E, and

(4.37a) $\quad \rho \sim 1 + \theta^{-1}[p_{10}(x,t_e)-T_{10}(x,t_e) + O(\tau)] + \ldots,$

(4.37b) $\quad Y \sim 1 + (\theta\beta)^{-1}[\{(\gamma-1)/\gamma\}p_{10}(x,t_e)-T_{10}(x,t_e)$

$\qquad\qquad + b(1-x/a) + O(\tau)] + \ldots\ .$

in OR. The constant b_1 appearing in (4.35b) and (4.36b) is given by

$$b_1 = \exp[\gamma b + \gamma \ell n \gamma - (\gamma-1)\ell n B_1]. \tag{4.38}$$

Observe that the BL-solutions (4.32), (4.33), (4.35) and (4.36) break down when $-\ell n \tau = O(\theta)$, signalling the end of the induction stage, and the onset of explosion. In contrast the OR-solutions, (4.34) and (4.37), suffer no disordering and in fact, become increasingly accurate as $\tau \to 0$.

5. The Type-B Explosion Stage

The nonuniformity just encountered decrees that further evolution in the boundary layer occur on the new time scale σ, defined by

$$\tau = e^{-\theta\sigma}. \tag{5.1}$$

For $\sigma = O(1)$ the limit $\theta \to \infty$ corresponds to a time interval of exponential brevity; its role in the evolution of thermal explosions was first recognized and exploited by Kassoy [8]. The two sublayers comprising the boundary layer must again be examined in turn. In fact, we shall find that as the boundary layers continue to shrink, an expanding void, or an intermediate region (denoted by IR in Figure 5), is created between the sublayer L_E and the outer region OR; this region begs a separate treatment.

5.1 The Interior Sublayer L_I

The spatial coordinate in this region remains s, now written as

$$s = x/\tau \equiv e^{\theta\sigma}\, x,$$

thereby expressing explicitly the continuous shrinkage of the region. In the (s,σ) variables eqns. (2.1) transform into

$$\theta^{-1}\rho_\sigma + s\rho_s + (\rho u)_s = 0, \tag{5.2a}$$

$$\rho[\theta^{-1}u_\sigma + su_s] + (1/\gamma)p_s + \rho u u_s = 0, \tag{5.2b}$$

(5.2c) $$\rho[\theta^{-1} T_\sigma + sT_s] - \{(\gamma-1)/\gamma\}[\theta^{-1} p_\sigma + sp_s] + u[\rho T_s - \{(\gamma-1)/\gamma\}p_s] = W,$$

(5.2d) $$\rho[\theta^{-1} Y_\sigma + sY_s] + u\rho Y_s = -(1/\beta)W,$$

(5.2e) $$p = \rho T,$$

where

(5.3) $$W = \theta^{-1} \rho Y \exp[\theta(1-\sigma-1/T)].$$

The boundary condition (2.2) is rewritten as

(5.4) $$u(0,\sigma) = 0.$$

At fixed s the solution must match with the induction zone as $\sigma \to 0$. To obtain the necessary conditions one applies the "explosion limit" σ fixed, $\theta \to \infty$ to the L_I-solution (4.32), (4.35) and gets

(5.5a) $$T \sim 1+\sigma - \theta^{-1} \ell n\gamma + \ldots + \delta[f_1(s) + \ldots],$$

(5.5b) $$p \sim 1+\sigma - \theta^{-1} \ell nB_1 + \ldots + \delta[g_1(s) + \ldots],$$

(5.5c) $$u \sim \delta[h_1(s) + \ldots],$$

(5.5d) $$\rho \sim 1 + \theta^{-1} \ell n(\gamma/B_1) + \ldots + \delta[g_1(s)-f_1(s) + \ldots],$$

(5.5e) $$Y \sim 1-\sigma/(\beta\gamma) + (\theta\beta\gamma)^{-1}\ell nb_1 + \ldots + \delta(\beta\gamma)^{-1}[(\gamma-1)g_1(s)-\gamma f_1(s)+ \ldots], \text{ as } \sigma \to 0.$$

Here,

(5.6) $$\delta = \theta^{-1} e^{-\sigma\theta\lambda},$$

where λ was defined in (4.14) and b_1 in (4.38). These conditions reveal that spatial variations in the explosion stage appear only at the (exponentially small) $O(\delta)$ level, thereby suggesting that the solution is spatially uniform to all algebraic orders in θ. In other words, the structure of the interior sublayer consists of an extremely weak chemico-acoustic field superimposed over a uniformly exploding atmosphere. Accordingly one seeks expansions of the form

$$u \sim \delta\, u_1(s,\sigma) + \ldots, \tag{5.7a}$$

$$\Phi \sim \Phi_0(\sigma;\theta) + \delta\, \Phi_1(s,\sigma) + \ldots, \text{ for } \Phi = T,\ p,\ \rho, \text{ and } Y, \tag{5.7b}$$

with the understanding that the Φ_0 contain all terms of algebraic orders. Substitution into (5.2) finds the Φ_0 satisfying the standard equations of constant-volume thermal explosion [8], i.e.,

$$\partial\rho_0/\partial\sigma = 0, \quad p_0 = \rho_0 T_0, \tag{5.8a}$$

$$(1/\gamma)\rho_0 \partial T_0/\partial\sigma = -\beta\rho_0 \partial Y_0/\partial\sigma = W_0 \equiv \rho_0 Y_0 \exp[\theta(1-\sigma-1/T_0)]. \tag{5.8b}$$

The solution, subject to the matching conditions (5.5), is

$$\Phi_0 \sim \Phi_{00} + \theta^{-1}\, \Phi_{01} + \ldots, \text{ for } \Phi = T,\ p,\ Y \text{ and } \rho, \tag{5.9a}$$

where

$$T_{00} = p_{00} = (1-\sigma)^{-1},\ Y_{00} = (1+\gamma\beta-T_{00})/(\gamma\beta),\ \rho_{00} = 1, \tag{5.9b}$$

$$T_{01} = -(1-\sigma)^{-2} \ell n\left[\gamma(1-\sigma)^2 Y_{00}\right],\ \rho_{01} = \ell n(\gamma/B_1), \tag{5.9c}$$

$$p_{01} = T_{01} + \rho_{01}/(1-\sigma),\ \beta\gamma Y_{01} = [\ell n(b_1/\gamma) - T_{01}]. \tag{5.9d}$$

The structure functions Φ_1 satisfy, to leading order, the equations

$$(5.10a) \qquad (s\partial/\partial s-\lambda)\rho_1 + \rho_0 \partial u_1/\partial s = 0,$$

$$(5.10b) \qquad \rho_0(s\partial/\partial s-\lambda)u_1 + (1/\gamma)\partial p_1/\partial s = 0,$$

$$(5.10c) \qquad (s\partial/\partial s-\lambda)[\rho_0 T_1-\{(\gamma-1)/\gamma\}p_1] = T_1 W_0/T_0^2,$$

$$(5.10d) \qquad \rho_0(s\partial/\partial s-\lambda)Y_1 = - T_1 W_0/(\beta T_0^2),$$

$$(5.10e) \qquad p_1 - \rho_0 T_1 - T_0 \rho_1 = 0,$$

where W_0 was defined in (5.8b). Replacement of T_0 and W_0 by their leading-order values from (5.9), followed by the use of the transformations

$$(5.11) \qquad u_1 = (1-\sigma)^{1/2}\,\hat{u}_1, \quad s = \hat{s}(1-\sigma)^{-1/2},$$

reduces the set (5.10) to

$$(5.12a) \qquad (\hat{s}\partial/\partial\hat{s}-\lambda)T_1 + (\gamma-1)\partial\hat{u}_1/\partial\hat{s} = T_1,$$

$$(5.12b) \qquad (\hat{s}\partial/\partial\hat{s}-\lambda)(T_1-p_1) - \partial\hat{u}_1/\partial\hat{s} = 0,$$

$$(5.12c) \qquad (\hat{s}\partial/\partial\hat{s}-\lambda)\hat{u}_1 + (1/\gamma)\partial p_1/\partial\hat{s} = 0,$$

$$(5.12d) \qquad \rho_1 = (p_1-T_1)/T_{00},$$

$$(5.12e) \qquad (\hat{s}\partial/\partial\hat{s}-\lambda)Y_1 + \{1/(\beta\gamma)\}T_1 = 0.$$

Eqns. (5.12a-c) are identical to (4.16a-c) if T_1, p_1, $\hat{u}_1$ and $\hat{s}$ in the former are identified, respectively, with f_1, g_1, h_1 and s in the latter. Following the arguments of section 4.1.1, therefore, one is led to the solution

(5.13a) $T_1 = [\hat{A}_1(\sigma)/A_1]f_1(\hat{s})$,

(5.13b) $p_1 = [\hat{A}_1(\sigma)/A_1]g_1(\hat{s})$

(5.13c) $u_1 = (1-\sigma)^{1/2}\,\hat{u}_1 = (1-\sigma)^{1/2}[\hat{A}_1(\sigma)/A_1]h_1(\hat{s})$,

where A_1 is the constant introduced earlier in (4.18). The amplitude function $\hat{A}_1(\sigma)$ is unknown at this stage, and will be determined by matching with the exterior sublayer. So far we only know its initial value as a result of matching with the induction solution (4.32), i.e.,

(5.14) $\hat{A}_1(0) = A_1$.

It is now a simple matter to solve (5.12d) for ρ_1, and compute Y_1 by integrating (5.12e) subject to the regularity requirement. The resulting expressions are

(5.15a) $\rho_1 = (1-\sigma)[\hat{A}_1(\sigma)/A_1][g_1(\hat{s})-f_1(\hat{s})]$,

(5.15b) $Y_1 = [\hat{A}_1(\sigma)/(\beta A_1)][\{(\gamma-1)/\gamma\}g_1(\hat{s})-f_1(\hat{s})]$.

Both the spatially uniform and the spatially-varying components of the expansions (5.7) are thus determined at leading orders, although the latter involve $\hat{A}_1(\sigma)$ which is still to be found. It is worth noting that the **spatial structure of the solution is essentially the same as it was at induction-stage blowup; the scalings (5.11) simply reflect the temporal evolution of the acoustic speed.**

As in section 4.1.1, the L_I-solution breaks down for large s,

the nonuniformity now occuring (see the expansion (4.21)) at $\theta\delta\hat{s}^{(2\gamma-1)/\gamma} = O(1)$. One is then led to the exterior sublayer.

5.2 The Exterior Sublayer L_E

Here the proper variables are ξ and σ where ξ is now related to x and $\hat{s}$ via the expressions

$$(5.16) \qquad \xi = x\, e^{\theta\sigma\gamma/(2\gamma-1)} = (1-\sigma)^{-1/2}\,\hat{s}\, e^{-\sigma\theta\mu},$$

and μ was defined in (4.23). In the new variables the full equations (2.1) read

$$(5.17a) \qquad \theta^{-1}\rho_\sigma + (1-\mu)\xi\rho_\xi + e^{-\theta\sigma\mu}(\rho u)_\xi = 0,$$

$$(5.17b) \qquad \rho e^{\theta\sigma\mu}[\theta^{-1}u_\sigma + (1-\mu)\xi u_\xi] + (1/\gamma)p_\xi + \rho u u_\xi = 0,$$

$$(5.17c) \qquad \rho[\theta^{-1}T_\sigma + (1-\mu)\xi T_\xi] - \{((\gamma-1)/\gamma\}[\theta^{-1}p_\sigma + (1-\mu)\xi p_\xi] + e^{-\theta\sigma\mu}u[\rho T_\xi - \{(\gamma-1)/\gamma\}p_\xi] = W,$$

$$(5.17d) \qquad \rho[\theta^{-1}Y_\sigma + (1-\mu)\xi Y_\xi] + e^{-\theta\sigma\mu}u\rho Y_\xi = -(1/\beta)W,$$

$$(5.17e) \qquad p = \rho T,$$

where W retains the definition (5.3). The solution is subject to the following matching conditions imposed by L_I:

$$(5.18a) \qquad T \sim T_{00} + \theta^{-1}[T_{01} - P\xi^{(2\gamma-1)/\gamma}] + \ldots,$$

$$(5.18b) \qquad p \sim T_{00} + \theta^{-1}[T_{01} + \rho_{01}/(1-\sigma) - P\xi^{(2\gamma-1)/\gamma}] + \ldots,$$

$$(5.18c) \qquad u \sim -e^{-\theta\sigma\mu}P\xi^{(\gamma-1)/\gamma}\big[A_h\mu\sigma + \theta^{-1}[A_h\ell n\{(1-\sigma)^{1/2}\xi\} + B_h]\big] + \ldots,$$

$$(5.18d) \qquad \rho \sim 1 + \theta^{-1}\rho_{01} + \ldots,$$

(5.18e) $$Y \sim Y_{00} + (\theta\beta\gamma)^{-1}\left[\ell n(b_1/\gamma) - T_{01} + P\xi^{(2\gamma-1)/\gamma}\right] + \ldots, \text{ as } \xi \to 0.$$

Here,

(5.19a) $$P(\sigma) = \alpha\hat{A}_1(\sigma)\ (1-\sigma)^{(2\gamma-1)/(2\gamma)},$$

with

(5.19b) $$P(0) = \alpha A_1,$$

from (5.14). In obtaining the conditions (5.18) we have employed the expansions (4.21) and the solution (5.13); the variables with double subscripts are the spatially homogeneous functions appearing in (5.9). It turns out that compliance with these conditions also ensures temporal matching with the induction stage. The L_E-solution is now sought in the form

(5.20a) $$T \sim T_{00} + \theta^{-1}\ \tilde{T}_1(\xi,\sigma) + \ldots,$$

(5.20b) $$p \sim T_{00} + \theta^{-1}\ \tilde{p}_1(\xi,\sigma) + \ldots,$$

(5.20c) $$u \sim e^{-\theta\sigma\mu}\left[\tilde{u}_0(\xi,\sigma) + \theta^{-1}\ \tilde{u}_1(\xi,\sigma) + \ldots\right],$$

(5.20d) $$Y \sim Y_{00} + \theta^{-1}\ \tilde{Y}_1(\xi,\sigma) + \ldots,$$

(5.20e) $$\rho \sim 1 + \theta^{-1}\ \rho_{01} + \ldots .$$

Substitution into (5.17) shows that (5.17a) is satisfied identically to $O(\theta^{-1})$. At O(1), (5.17b) reduces to

$$(1-\mu)\xi\partial\tilde{u}_0/\partial\xi - \mu\tilde{u}_0 = 0$$

whose solution subject to the matching requirement (5.18c) is

$$\tilde{u}_0 = \{(\gamma-1)/\gamma^2\}\sigma P\xi^{(\gamma-1)/\gamma}. \tag{5.21}$$

At $O(\theta^{-1})$, (5.17e) yields

$$\tilde{p}_1 = \tilde{T}_1 + \rho_{01}/(1-\sigma), \tag{5.22}$$

while (5.17c) reduces to

$$(1-\sigma)^{-2} + (1-\mu)\xi\partial\tilde{T}_1/\partial\xi - \{(\gamma-1)/\gamma\}\left[(1-\sigma)^{-2} + (1-\mu)\xi\partial\tilde{p}_1/\partial\xi\right] = Y_{00}\exp[(1-\sigma)^2\tilde{T}_1],$$

and, in view of (5.22), simplifies further to

$$(1-\sigma)^{-2} + (1-\mu)\xi\partial\tilde{T}_1/\partial\xi = \gamma Y_{00}\exp[(1-\sigma)^2\tilde{T}_1]. \tag{5.23}$$

Its solution, consistent with the matching condition (5.18a), is

$$\tilde{T}_1 = T_{01} - (1-\sigma)^{-2}\ln\left[1 + (1-\sigma)^2 P\xi^{(2\gamma-1)/\gamma}\right]. \tag{5.24}$$

With $\tilde{T}_1$ known, (5.22) defines $\tilde{p}_1$. In order to determine $\tilde{Y}_1$ consider (5.17d) at $O(\theta^{-1})$; it yields

$$-(\beta\gamma)^{-1}(1-\sigma)^{-2} + (1-\mu)\xi\partial\tilde{Y}_1/\partial\xi$$

$$= (-1/\beta)Y_{00}\exp[(1-\sigma)^2\tilde{T}_1].$$

When linearly combined with (5.23) the above equation leads to

$$\partial[\tilde{T}_1 + \beta\gamma\tilde{Y}_1]/\partial\xi = 0.$$

The matching condition (5.18e) then provides the following expression for Y_1:

$$\beta\gamma\tilde{Y}_1 = \ell n(b_1/\gamma) - \tilde{T}_1. \tag{5.25}$$

It now remains to determine $\tilde{u}_1$, and the function $P(\sigma)$ (or, equivalently, $\hat{A}_1(\sigma)$). Both are obtainable from (5.17b) which, at $O(\theta^{-1})$, reads

$$(1-\mu)\xi\partial\tilde{u}_1/\partial\xi - \mu\tilde{u}_1 = -\partial\tilde{u}_0/\partial\sigma - (1/\gamma)\partial\tilde{p}_1/\partial\xi. \tag{5.26}$$

With $\tilde{u}_0$ and $\tilde{p}_1$ known (see (5.21), (5.22) and (5.24)), the general solution of the above equation can be written as

$$\tilde{u}_1 = \{(2\gamma-1)/\gamma\}\xi^{(\gamma-1)/\gamma}\Big[K - \{(\gamma-1)/\gamma^2\}(\sigma P)'\ell n\xi + (P/\gamma)\ell n[\xi^{(2\gamma-1)/\gamma}/\{1+P(1-\sigma)^2\xi^{(2\gamma-1)/\gamma}\}]\Big], \tag{5.27}$$

where $K(\sigma)$ is the integration "constant". As $\xi \to 0$, $\tilde{u}_1$ has the asymptotic behavior

$$\tilde{u}_1 \sim \{(2\gamma-1)/\gamma\}\xi^{(\gamma-1)/\gamma}\Big[[-\{(\gamma-1)/\gamma^2\}(\sigma P)'$$ (5.28)

$$+ \{(2\gamma-1)/\gamma^2\}P]\ell n\xi + K] + \ldots ,$$

which must agree with the $O(\theta^{-1})$ term in (5.18c). Matching the $\ell n\xi$ terms yields the differential equation

$$[\sigma P(\sigma)]' = P$$

whose solution, subject to (5.19b), is

$$P = \alpha A_1 , \tag{5.29a}$$

or, equivalently,

$$\hat{A}_1 = A_1(1-\sigma)^{-(2\gamma-1)/(2\gamma)} . \tag{5.29b}$$

With P determined, matching of the ξ-independent terms in (5.28) and (5.18c) yields K:

$$K = (\alpha A_1/\gamma)[(1/2)\ell n(1-\sigma) - \{\gamma^2/(2\gamma-1)\}B_h], \tag{5.30}$$

where the constant B_h was defined in eqn. (4.22). The L_E-solution at the explosion stage is thus complete.

It is instructive to compare the solutions in the two sublayers. In each the background field is that of a spatially homogeneous thermal explosion, but the superimposed spatially-varying field is quite different, both in amplitude and structure. In L_I the spatial component is exponentially small in amplitude but has a

chemico-acoustic character; all disturbances to the background homogeneous field are of the same size. In L_E the spatial variations in T, Y and p are $O(\theta^{-1})$, while those in u and ρ are exponentially small, i.e., the evolution is essentially due to constant-volume chemical amplification of a spatially-non-uniform field, with gasdynamics playing a very minor role.

As σ increases, T and p increase and Y decreases, in both the sublayers. Eventually, p and T peak when Y_{00}, the leading term in Y, vanishes. This happens at (see (5.9))

$$\sigma = \beta\gamma/(1+\beta\gamma), \tag{5.31a}$$

and the peak values are

$$T \sim 1+\beta\gamma, \quad p \sim 1+\beta\gamma. \tag{5.31b}$$

At the same time, the $O(\theta^{-1})$ term (in T, say; see (5.20a), (5.24) and (5.9c)) develops a logarithmic singularity, indicating breakdown of the solution and the end of the explosion stage.

5.3 The Outer Region OR

This region remains essentially stationary, and hence plays no role during the explosion stage. For the sake of completeness, we give below the asymptotic form of the outer solution as $x \to 0$; these expressions are determined by combining (4.31) and (4.34):

$$T \sim 1 + \theta^{-1}\left[-\{(2\gamma-1)/\gamma\}\ell n x - \ell n(A_1\alpha\gamma)\right] + \ldots, \tag{5.32a}$$

$$(5.32b) \qquad p \sim 1 + \theta^{-1}\left[-\{(2\gamma-1)/\gamma\}\ell n x - \ell n(A_1 \alpha B_1)\right] + \ldots,$$

$$(5.32c) \qquad u \sim \theta^{-1} A_1 \alpha\, x^{(\gamma-1)/\gamma}\left[\{(2\gamma-1)/\gamma^2\}[\{-(\gamma-1)/\gamma\}\ell n x - \ell n(A_1\alpha)] - B_h\right] + \ldots .$$

Similar expressions can be written for ρ and Y. The important point to note is that this solution is unmatchable with that in L_E; for example, to leading order, T is 1 in OR and $1/(1-\sigma)$ in L_E. The reason is the emergence of the intermediate region IR in Figure 5, created by the receding boundary layer. In this region T must vary, at leading order, from the outer value 1 to the inner value $1/(1-\sigma)$.

5.4 The Intermediate Region IR

This region, because of its passive character, will only be described very briefly. It is governed by the variables σ and X, where X is defined by

$$(5.33) \qquad x = e^{-\theta X}.$$

Matching with the neighboring regions is carried out at fixed σ, by setting

$$X = -\theta^{-1}\, \ell n x$$

as one approaches the outer region, and

$$X = \sigma(1-\mu) - \theta^{-1}\, \ell n \xi,$$

as the boundary layer is approached. Therefore the range of X is

(5.34) $\quad 0 < X < \sigma(1-\mu);$

recall that μ was defined in (4.23). From (5.20) one can easily conclude that leading-order matching with L_E requires

(5.35a) $\quad T \sim 1/(1-\sigma) + \ldots$, as $X \to \sigma(1-\mu)$,

with analogous expressions for p and Y, while

(5.35b) $\quad \rho \sim 1$, $u \sim e^{-\theta X(\gamma-1)/\gamma} \{(\gamma-1)/\gamma^2\} A_1 \alpha\sigma.$

Therefore the solution is sought in the form

(5.36a) $\quad \Phi \sim \Phi^0 + \ldots$, for $\Phi = T$, p, ρ and Y,

and

(5.36b) $\quad u \sim e^{-\theta X(\gamma-1)/\gamma} u^0 + \ldots$.

In the (X,σ) variables the full equations (2.1) read

$$\rho_\sigma - (u\rho)_X e^{-\theta(\sigma-X)} = 0,$$
$$\rho\left[u_\sigma - uu_X e^{-\theta(\sigma-X)}\right] - (1/\gamma)p_X e^{-\theta(\sigma-X)} = 0,$$
$$\rho\left[T_\sigma - uT_X e^{-\theta(\sigma-X)}\right] - \{(\gamma-1)/\gamma\}\left[p_\sigma - up_X e^{-\theta(\sigma-X)}\right] = W,$$
$$\rho\left[Y_\sigma - uY_X e^{-\theta(\sigma-X)}\right] = -(1/\beta)W,$$

$$p = \rho T,$$

where W retains the definition (5.3). Clearly, the solution is stationary, i.e., independent of σ to all algebraic orders. Specifically, the reaction term W is exponentially small since one expects $T < 1/(1-\sigma)$. The leading-order terms can then be determined simply by appealing to the matching conditions (5.35), and one finds that

$$(5.37a) \qquad T^0 = 1/[1-(1-\mu)^{-1}X],$$

with analogous expressions for p and Y, while

$$(5.37b) \qquad \rho^0 = 1, \; u^0 = \{(\gamma-1)/\gamma^2\}A_1\alpha\,(1-\mu)^{-1}X.$$

It is a simple matter to check that the above solution also matches with the outer expansions (5.32) as $X \to 0$.

The analysis of the Type-B explosion is thus complete.

6. The Type-I Explosion

In this section details are largely omitted and emphasis is on the results, since the treatment follows closely the Type-B analysis just concluded.

6.1 The Induction Stage

Figures 7(a-d) display the numerical solution of the induction problem. The graphs are self-explanatory. Similarity with Figures

2(a-d) is obvious, but two points of contrast are noteworthy. First, the temperature profile now has a rounded peak. Second, the boundary layer is thicker; this can be seen more clearly in Figure 8, where $T_1(x,t)/T_1(0,t)$ is plotted at the last successful time step for each of the two cases.

The boundary layer retains the form (4.8) and a two-sublayer structure emerges once again. The expansions are

$$(6.1a)\qquad T \sim 1 + \theta^{-1}\left[-\ell n(\gamma\tau) - \tau\ell n\tau\,\{(\gamma-1)/\gamma\}A_1 + \tau\,\{-A_1 s^2 + A_2\} + \ldots\right] + \ldots,$$

$$(6.1b)\qquad p \sim 1 + \theta^{-1}\left[-\ell n(B_1\tau) - \tau\ell n\tau\,\{(\gamma+1)/\gamma\}A_1 + \tau\,[-A_1 s^2 + \{(\gamma+1)/(\gamma-1)\}A_2 + A_1/\gamma] + \ldots\right] + \ldots,$$

$$(6.1c)\qquad u \sim \theta^{-1}\left[\tau\ell n\tau\,\{-2A_1 s/\gamma\} + \tau\,[2A_2/(\gamma-1) - A_1/\gamma]s + \ldots\right] + \ldots$$

in L_I, and

$$(6.2a)\qquad T \sim 1 + \theta^{-1}\left[-\ell n(\gamma\tau) - \ell n(1+A_1\zeta^2) + \ldots\right] + \ldots,$$

$$(6.2b)\qquad p \sim 1 + \theta^{-1}\left[-\ell n(B_1\tau) - \ell n(1+A_1\zeta^2) + \ldots\right] + \ldots,$$

$$(6.2c)\qquad u \sim \theta^{-1}\left[\tau^{1/2}\ell n\tau\,\{-(2/\gamma)A_1\zeta\} + \tau^{1/2}\,[-(2/\gamma)A_1\zeta\,\ell n(1+A_1\zeta^2) + \{2A_2/(\gamma-1) - A_1/\gamma\}\zeta] + \ldots\right] + \ldots,$$

in L_E. The coefficients A_1, A_2 and B_1 are to be determined by matching with the outer solution as before. The spatial coordinate ζ in L_E is defined by

$$(6.3)\qquad \zeta = x/\tau^{1/2},$$

implying that the boundary layer is now $O(\varepsilon^{1/2})$ thick, and hence thicker than the $O(\varepsilon^{\gamma/(2\gamma-1)})$ Type-B layer. The finding of Figure 8 is thus confirmed.

It turns out further that the L_E-solution is uniformly valid all the way to $\zeta = 0$, so that the interior sublayer is, in fact, superfluous.

For smooth merging with the boundary layer the outer, numerically computed solution is required to have the asymptotic form

$$T \sim 1 + \theta^{-1}\,[-2\ell nx - \ell n(\gamma A_1) + \ldots] + \ldots, \tag{6.4a}$$

$$p \sim 1 + \theta^{-1}\,[-2\ell nx - \ell n(A_1 B_1) + \ldots] + \ldots, \tag{6.4b}$$

$$u \sim \theta^{-1}\,[-4(A_1/\gamma)x\ell nx + \{-2(A_1/\gamma)\ell nA_1 + 2A_2/(\gamma-1) - A_1/\gamma\}x + \ldots] + \ldots, \text{ as } x \to 0. \tag{6.4c}$$

This behavior was confirmed, and the constants A_1, A_2 and B_1 computed, by comparing the numerical solution with the above expansions. The remaining variables ρ_1 and Y_1 can be determined as before, by appealing to the first member of (3.2c), and (3.2d).

6.2 The Explosion Stage

The analysis proceeds as in section 5.2. The appropriate coordinates are σ and ζ, and the requirement of matching with L_I is replaced by the condition of regularity at $\zeta = 0$. The solution turns out to be

$$T \sim T_{00} + \theta^{-1}\left[T_{01} - (1-\sigma)^{-2}\ell n\{1+A_1\zeta^2\}\right] + \ldots, \tag{6.5a}$$

$$p \sim T_{00} + \theta^{-1}\left[T_{01} - (1-\sigma)^{-2}\ell n\{1+A_1\zeta^2\} + \rho_{01}/(1-\sigma)\right] + \ldots, \tag{6.5b}$$

$$u \sim e^{-\theta\sigma/2}\left[\Xi A_1\zeta\sigma/\{\gamma(1-\sigma)\}\right] + \ldots \tag{6.5c}$$

$$\rho \sim 1 + \theta^{-1}\rho_{01} + \ldots, \tag{6.5d}$$

$$Y \sim Y_{00} + (\theta\beta\gamma)^{-1}\left[\ell n(b_1/\gamma) - T_{01} + (1-\sigma)^{-2}\ell n\{1+A_1\zeta^2\}\right] + \ldots, \tag{6.5e}$$

where the constant b_1 appearing in (6.5e) was defined in (4.38). The doubly subscripted quantities correspond to the spatially homogeneous explosion, and were introduced in (5.9). The explosion stage peaks just as it did for Type-B, and the remarks at the end of section 5.2 remain valid. Finally, the IR-analysis of section 5.4 carries over, with obvious modifications.

7. Concluding Remarks

The spatial structure and temporal evolution of a localized thermal explosion in a confined gas have been described mathematically. Localization, rather than a spatially uniform explosion, occurs as a result of system nonhomogeneities, here modelled by a slightly nonuniform initial temperature. Attention is confined to what may be called the fast-reaction limit, characterized by the initial induction time of the reaction being comparable to the initial acoustic time across the vessel, so that diffusion plays no role. This limit can be achieved if the initial temperature of the unreacted gas has been raised to a sufficiently high level, perhaps by the passage of a strong shock. By contrast, the slow-reaction limit would correspond to the induction time and the conduction time being of the same order. The latter problem was the subject of Poland and Kassoy's investigation [6].

The explosion is shown to develop in two distinct stages. The first stage is induction, characterized by small perturbations about a spatially uniform state, where the primary interaction is between linearized acoustics and weak but nonlinear chemical heating. Chemical amplification leads to localized thermal runaway, or blowup of the perturbations, at a time and location determined by the initial and boundary conditions. The spatial structure at blowup is self-similar, differing slightly depending upon whether the runaway site is at the boundary or in the interior of the domain.

Induction is followed by explosion, characterized by O(1)

variations in the state of the gas. The characteristic chemical time plunges dramatically. The acoustic time drops as well, but not nearly in the same proportion, so that explosion is dominated by chemical heating. There is no time for expansion, with the result that changes in the velocity and density fields are negligible. Thus the gas explodes locally at essentially constant-volume conditions, with little change in the spatial structure that it inherited at runaway. (Analysis in the Appendix shows that if thermal expansion is admitted, the corresponding spatial structure is necessarily singular.) The explosion stage ends when temperature and pressure within the explosion have peaked, the final values being exactly the same, to leading order, as in the spatially homogeneous case. The subsequent expansion of the hot, highly compressed gas, and the eventual development of a blast wave, are currently under study.

Acknowledgements

Part of this work was carried out during A. K. Kapila's visits to ICASE and the Los Alamos National Laboratories. The hospitality and financial support of the two institutions is gratefully acknowledged.

REFERENCES

1. Urtiew, P. A. and Oppenheim, A. K. (1966) Experimental observations of the transition to detonation in an explosive gas, Proc. Roy. Soc. A 295, 13-28.

2. Zajac, L. J. and Oppenheim, A. K. (1971) Dynamics of an explosive reaction center, AIAA J. 9, 545-553

3. Meyer, J. W. and Oppenheim, A. K. (1972) Dynamic response of a plane-symmetrical exothermic reaction center, AIAA J. 10, 1509-1513.

4. Clarke, J. F. and Cant, R. S. (1984) Non-steady gasdynamic effects in the induction domain behind a strong shock wave, Progress in Aeronautics and Astronautics 95, 142-163.

5. Jackson, T. L. and Kapila, A. K. (1985) Shock-induced thermal runaway, SIAM J. Appl. Math. 45, 130-137.

6. Poland, J. and Kassoy, D. R. (1983) The induction period of a thermal explosion in a gas between infinite parallel plates, Combustion and Flame 50, 259-274.

7. Williams, F. A. (1985) **Combustion Theory**, Benjamin Cummings Publishing Company.

8. Kassoy, D. R. (1976) Extremely rapid transient phenomena in combustion, ignition and explosion, in **Asymptotic Methods and Singular Perturbations**, R. E. O'Malley, Jr., ed.,SIAM-AMS Proceedings 10, 61-72.

Appendix

The setup (4.8), employed in the text for analyzing the spatial structure of blowup, is based on the numerical observation that both T_1 and p_1 exhibit identical, $-\ell n\tau$ behavior as $\tau \to 0$. This observation, found to hold for all the numerical runs undertaken, implies that blowup is a constant-volume process, since density perturbation $\rho_1 = p_1 - T_1$ remains bounded.

Let us now consider the possibility that for some initial conditions, blowup lies partway between a constant-volume and a constant-pressure process, and ask whether a self-similar structure consistent with this notion exists. Accordingly, we replace (4.8) by

$$T_1 \sim -\ell n\tau + f_0(s) + \ldots, \tag{A.1a}$$

$$p_1 \sim -\Lambda\ell n\tau + g_0(s) + \ldots, \tag{A.1b}$$

$$u_1 \sim h_0(s) + \ldots, \tag{A.1c}$$

where

$$0 < \Lambda < 1.$$

The case $\Lambda = 0$ corresponds to a constant-pressure situation, and $\Lambda = 1$ to the constant-volume case already discussed. Substitution into (4.7), followed by some rearrangement, yields the leading-order structure equations

(A.2a) $$s(1-s^2)f_0' + [1-s^2-\{((\gamma-1)/\gamma)\Lambda] = (1-\gamma s^2)\exp f_0,$$

(A.2b) $$(1-s^2)g_0' = s[\Lambda-\gamma\exp f_0],$$

(A.2c) $$\gamma(1-s^2)h_0' = \gamma\exp f_0 - \Lambda.$$

The transformation

(A.3) $$f_0 = -\ell nF$$

reduces (A.2a) to the linear equation

(A.4) $$s(1-s^2)F' - [1-s^2-\{((\gamma-1)/\gamma)\Lambda]F = 1-\gamma s^2.$$

Once F is known, f_0, g_0 and h_0 can be computed sequentially from (A.3) and (A.2b,c).

Equation (A.4) has singular points at s = 0 and 1. It can be shown that in general integration can remove at most one singularity, thereby yielding solutions which are singular either at 0 or at 1. Such solutions can evolve only from very special, singular initial conditions, and are therefore unacceptable if the initial data are smooth. The only regular solution is the constant

$$F = \gamma,$$

which requires

$$\Lambda = 1,$$

corresponding to the constant-volume blowup already discussed.

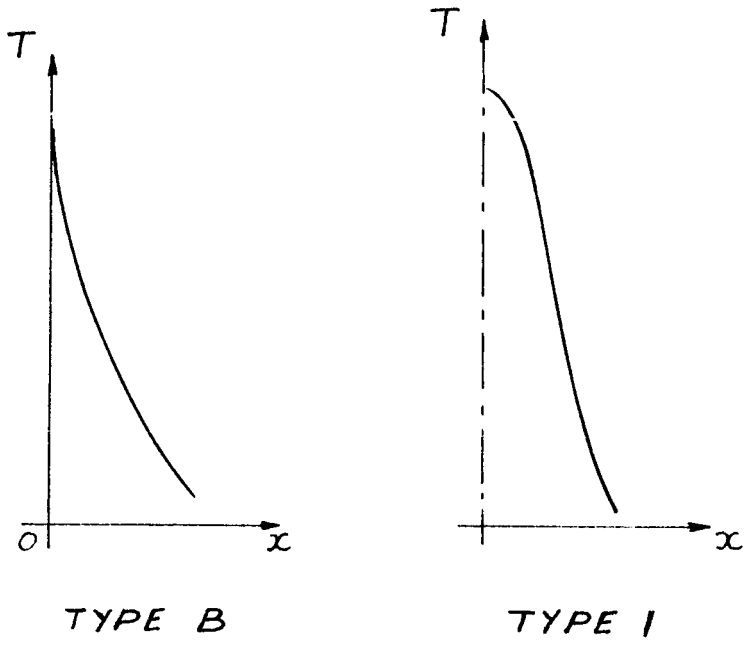

Figure 1

A scematic of the temperature profiles for the Type-B (sharp peaked) and the Type-I (round-peaked) explosion.

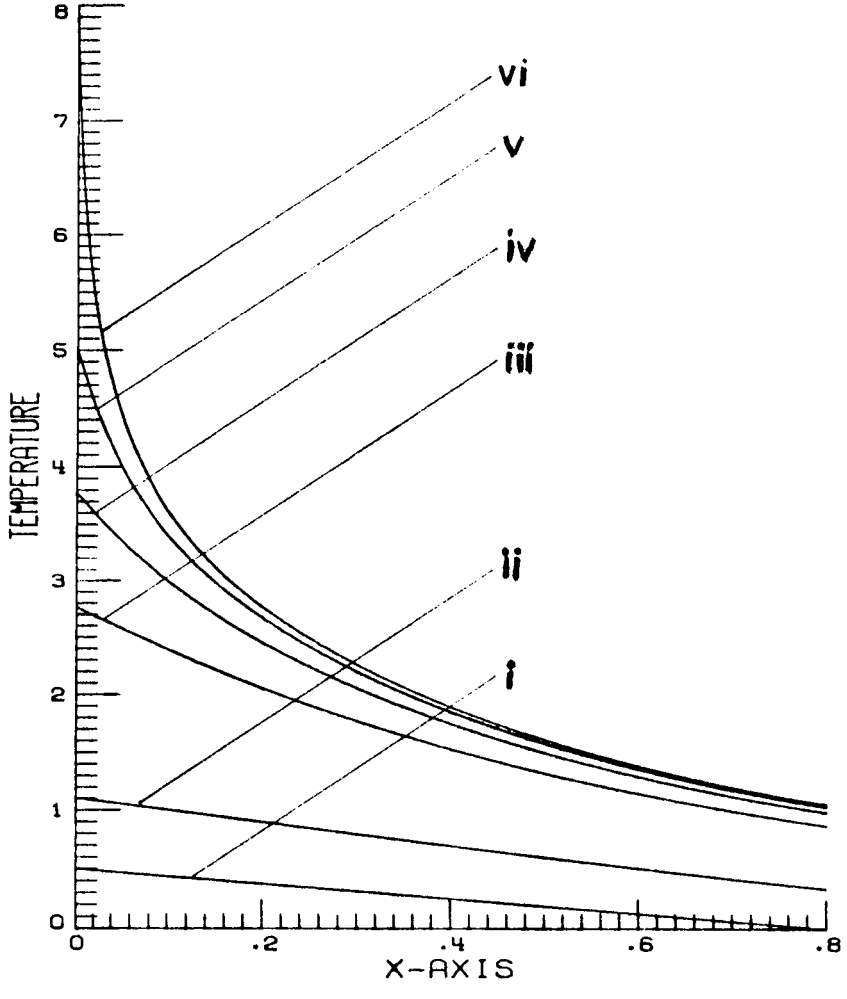

Figure 2(a)

Type-B induction-stage profiles for (a) T_1, (b) p_1, (c) u_1 and (d) ρ_1. The profiles are plotted at (i) t=0, (ii) t=0.2, (iii) t=0.4, (iv) t=0.43, (v) t=0.442, (vi) t=0.44625. Estimate of blowup time is t_e = 0.446890.

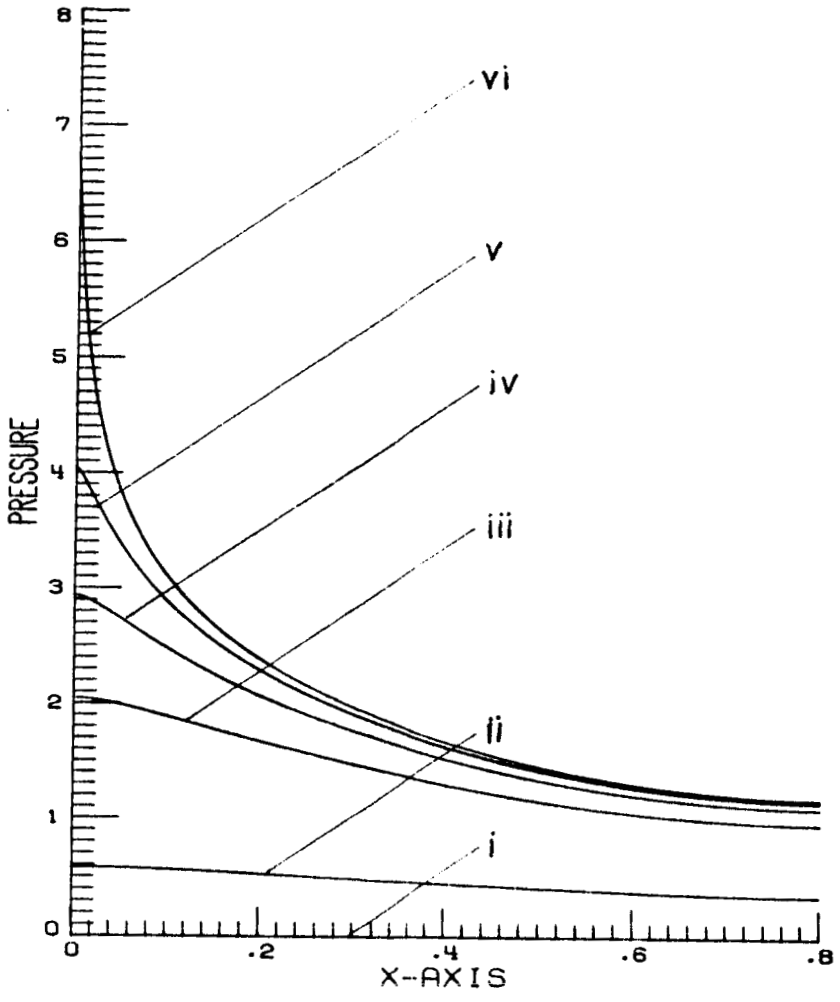

Figure 2(b)

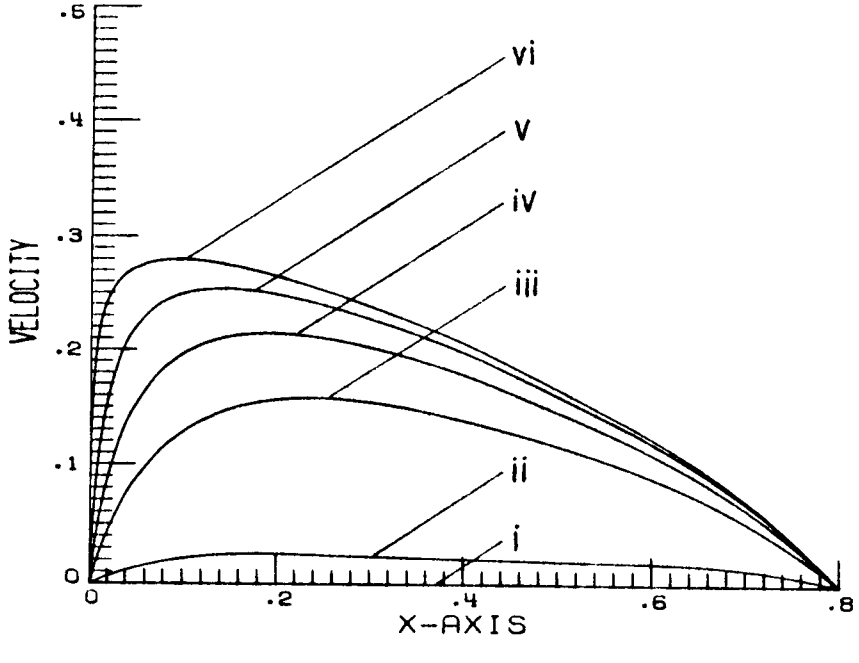

Figure 2(c)

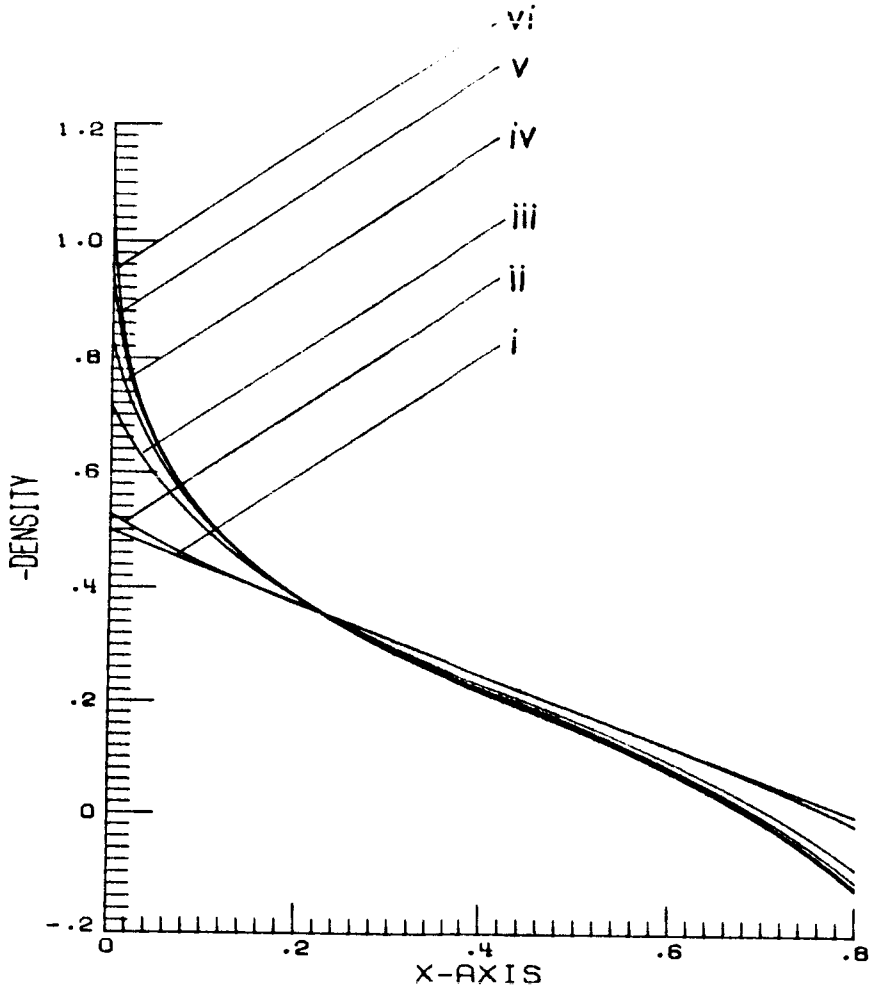

Figure 2(d)

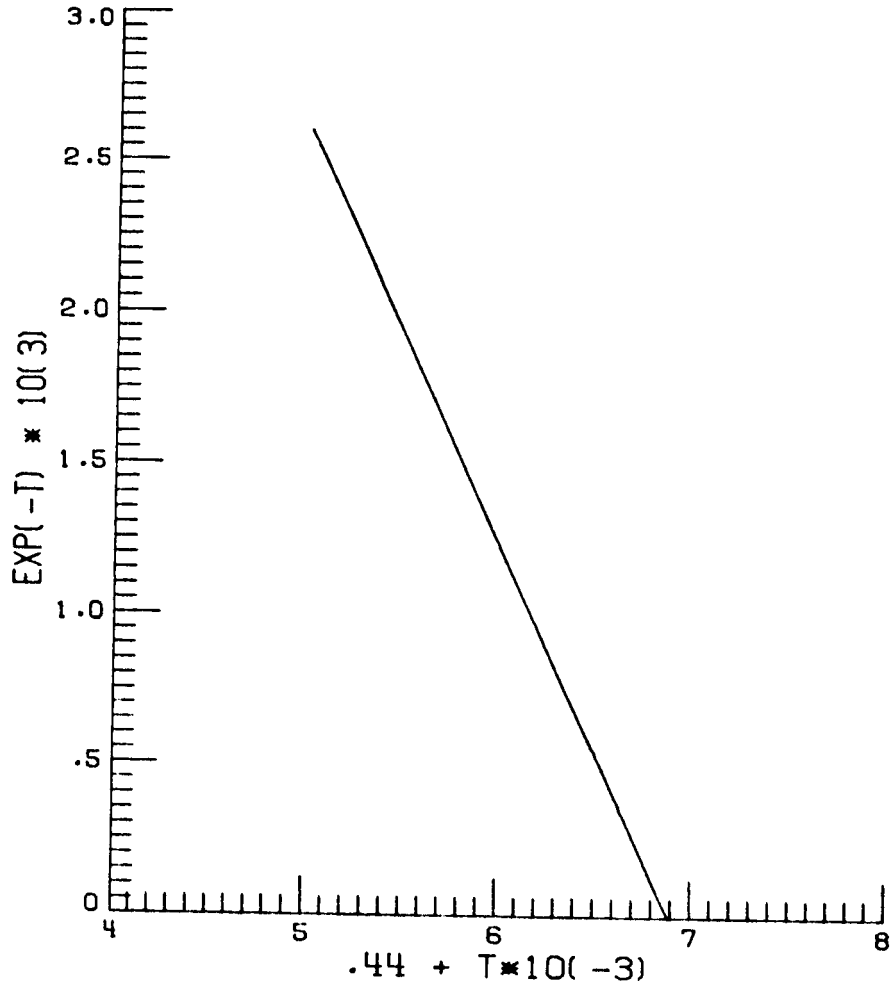

Figure 3

Plot of $\exp[-T_1(0,t)]$ for Type-B problem.

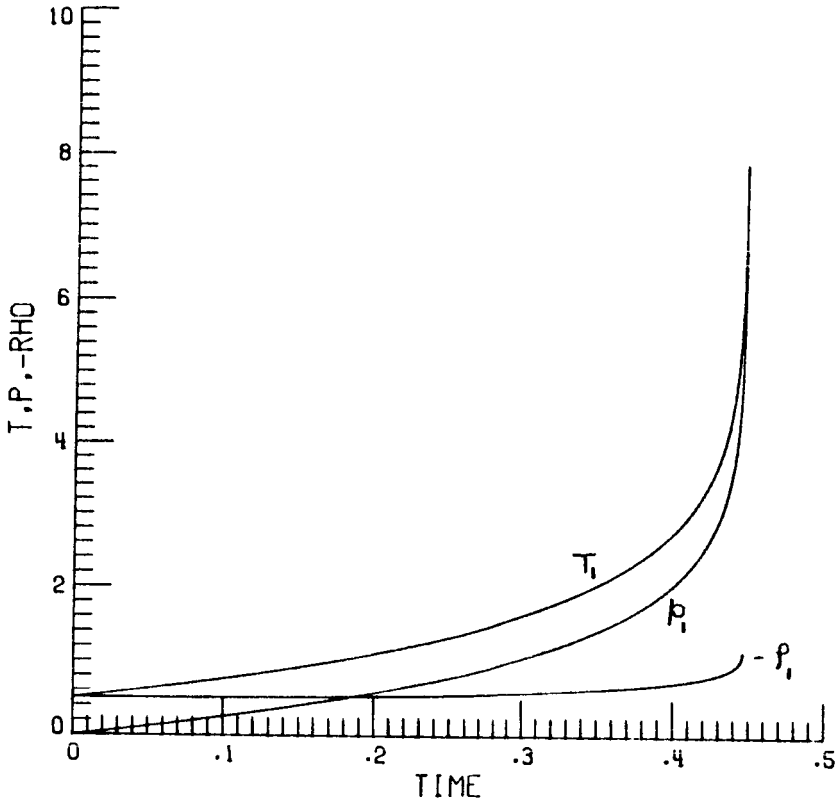

Figure 4

Type-B plots of $T_1(0,t)$, $p_1(0,t)$ and $\rho_1(0,t)$.

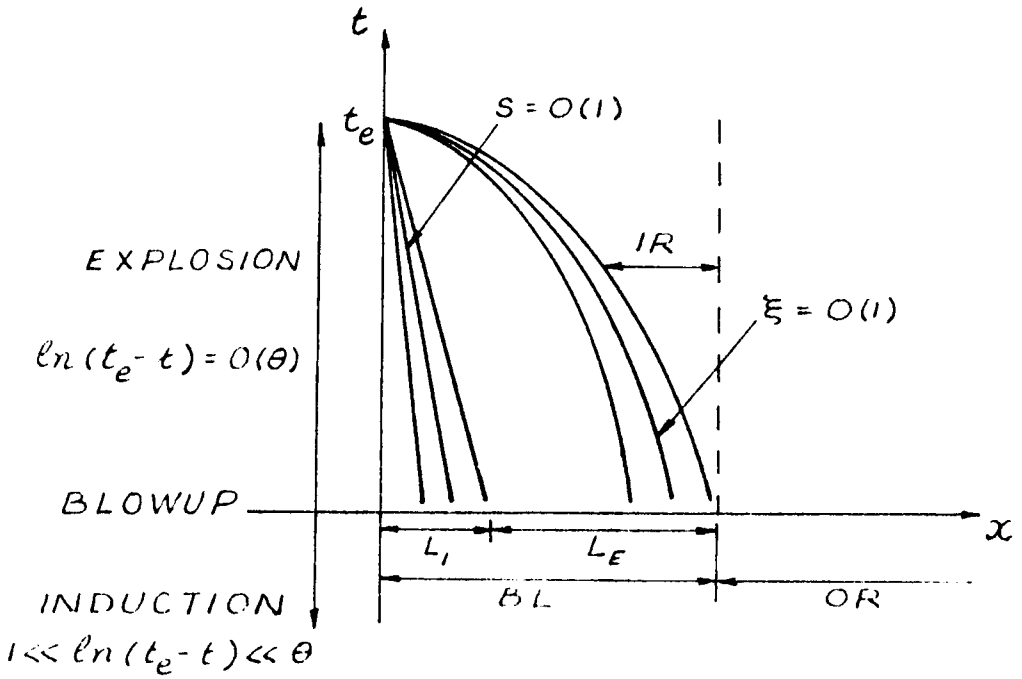

Figure 5

A schematic of the spatial zones at and beyond blowup. BL: Boundary Layer, L_I: Interior Sublayer, L_E: Exterior Sublayer, OR: Outer Region, IR: Intermediate Region. Not to scale (The t-scale is cosiderably stretched).

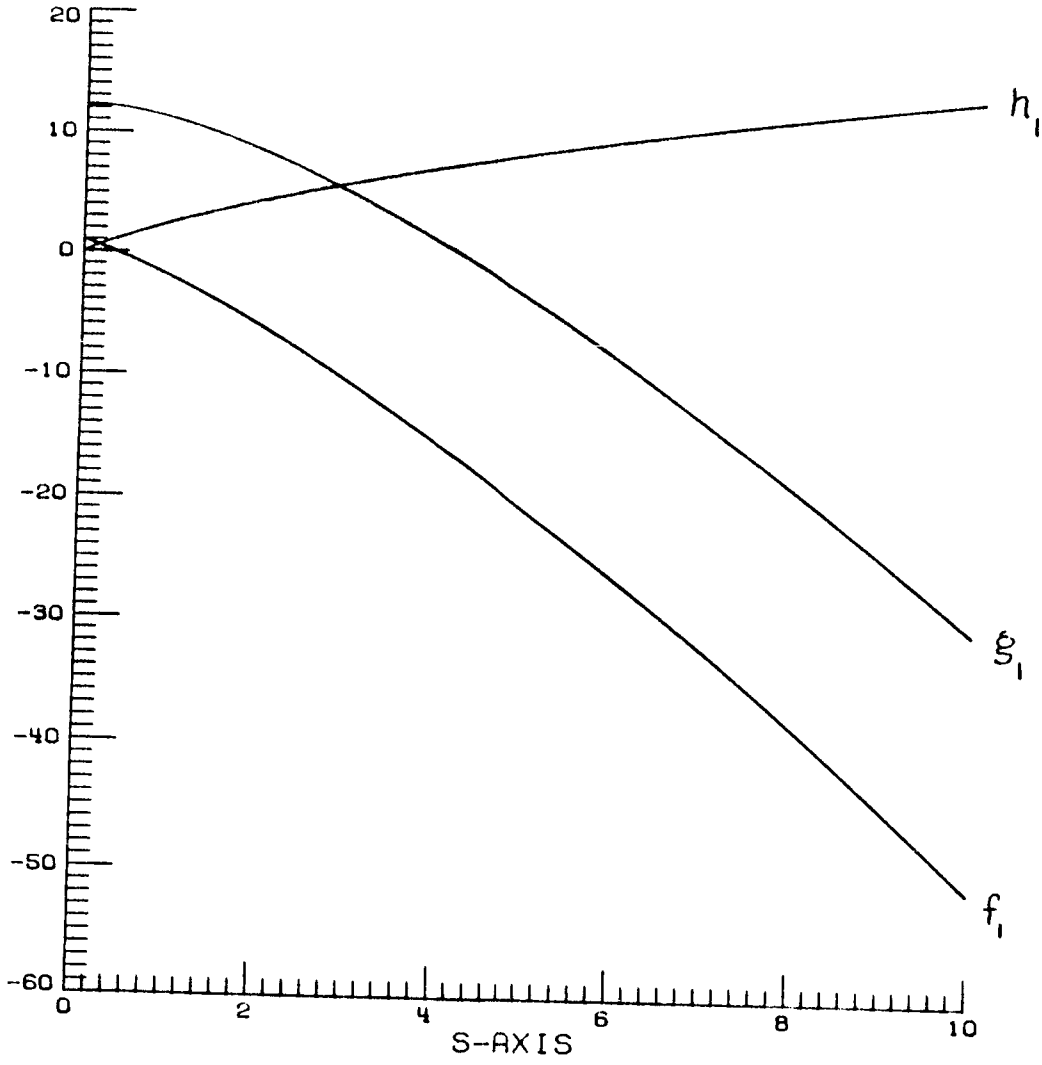

Figure 6

Profiles of structure functions f_1, g_1 and h_1 for $f_1(0) = 1$.

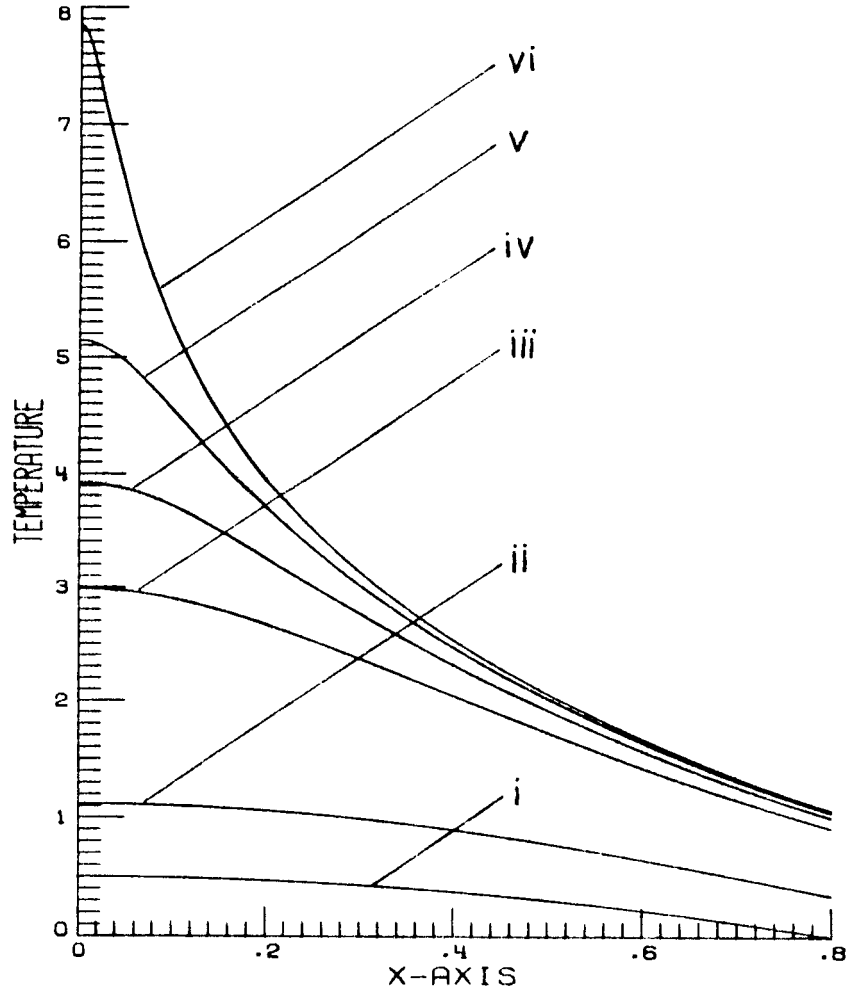

Figure 7(a)

Type-I induction-stage profiles for (a) T_1, (b) p_1, (c) u_1 and (d) ρ_1. The profiles are plotted at (i) t=0, (ii) t=0.2, (iii) t=0.4, (iv) t=0.422, (v) t=0.432, (v1) t=0.435875. Estimate of blowup time is t_e = 0.435880.

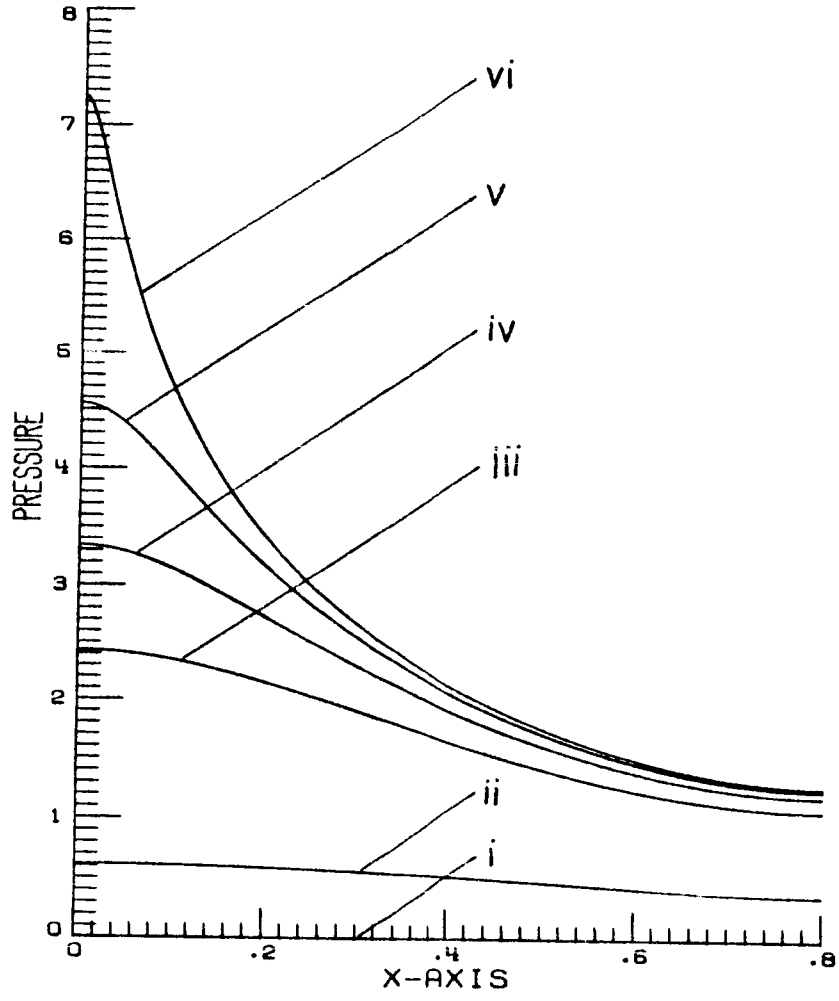

Figure 7(b)

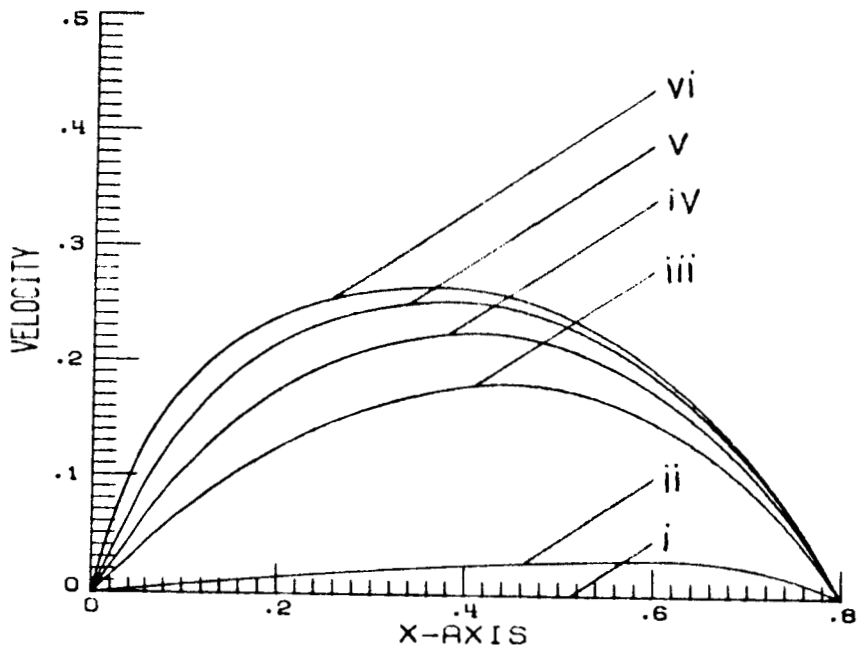

Figure 7(c)

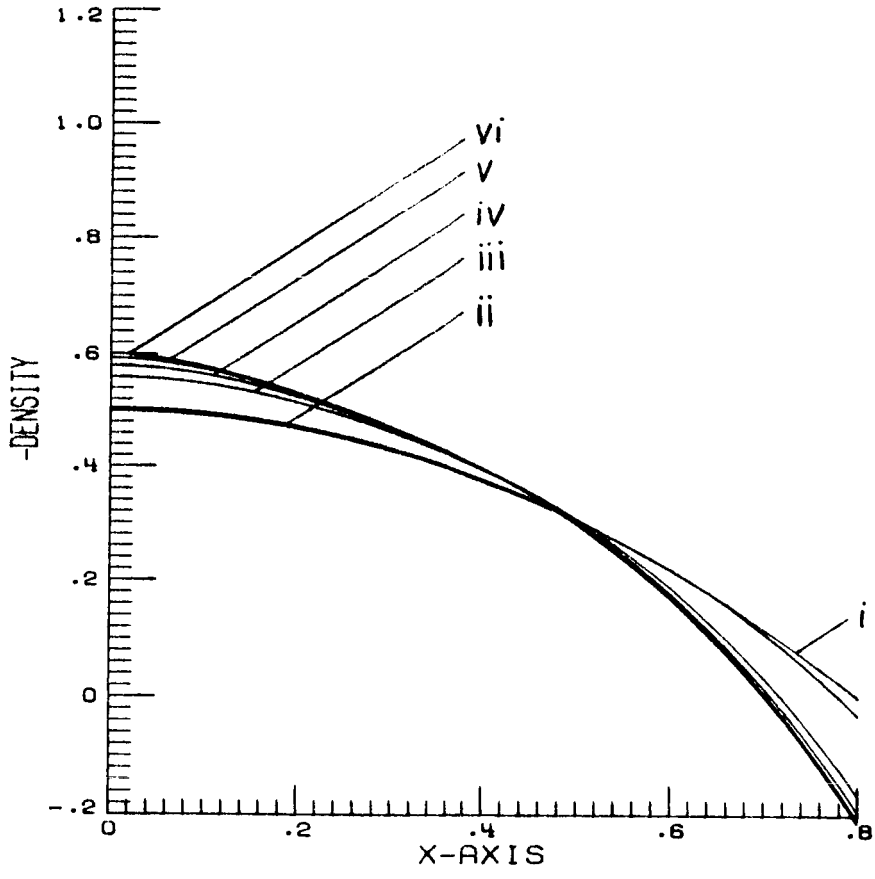

Figure 7(d)

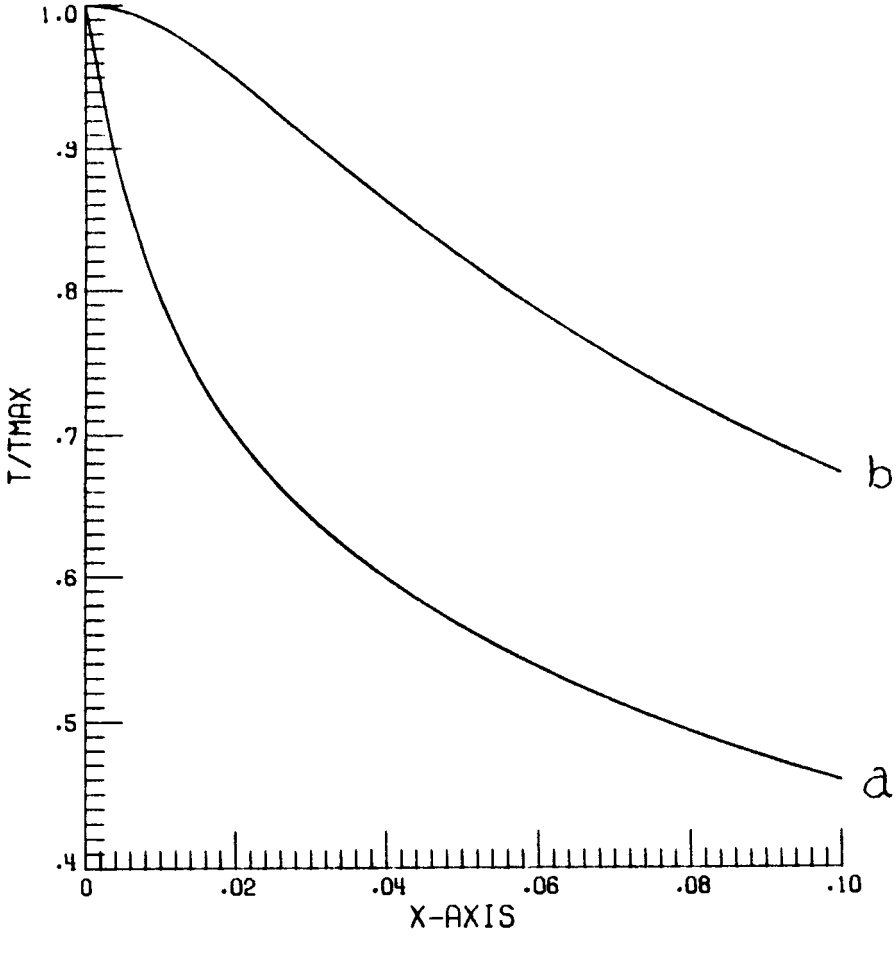

Figure 8

Plots of $T_1(x,t)/T_1(0,t)$ at the last integration step for (a) Type B, and (b) Type I.

Standard Bibliographic Page

1. Report No. NASA CR-178231 ICASE Report No. 87-2	2. Government Accession No.	3. Recipient's Catalog No.
4. Title and Subtitle EVOLUTION OF A LOCALIZED THERMAL EXPLOSION IN A REACTIVE GAS		5. Report Date January 1987 6. Performing Organization Code
7. Author(s) T. L. Jackson, A. K. Kapila, and D. S. Stewart		8. Performing Organization Report No. 87-2
9. Performing Organization Name and Address Institute for Computer Applications in Science and Engineering Mail Stop 132C, NASA Langley Research Center Hampton, VA 23665-5225		10. Work Unit No. 11. Contract or Grant No. NAS1-18107
12. Sponsoring Agency Name and Address National Aeronautics and Space Administration Washington, D.C. 20546		13. Type of Report and Period Covered Contractor Report 14. Sponsoring Agency Code 505-90-21-01

15. Supplementary Notes

Langley Technical Monitor:
J. C. South

Submitted to SIAM J. of Applied Math.

Final Report

16. Abstract

Experimental observations of ignition in premixed gaseous reactants indicate that perfectly homogeneous initiation is practically unrealizable. Instead, combustion first sets in, as a rule, at small, discrete sites where inherent inhomogeneities cause chemical activity to proceed preferentially and lead to localized explosions. Combustion waves propagating away from these "hot spots" or "reaction centers" eventually envelope the remaining bulk.

This study examines the spatial structure and temporal evolution of a hot spot for a model involving Arrhenius kinetics. The hot spot, characterized by peaks in pressure and temperature with little diminution in local density, is shown to have one of two possible self-similar structures. The analysis employs a combination of asymptotics and numerics, and terminates when pressure and temperature in the explosion have peaked.

17. Key Words (Suggested by Authors(s))	18. Distribution Statement
thermal explosion, asymptotics, reactive gas	59 - Mathematical and Computer Sciences Unclassified - unlimited

19. Security Classif.(of this report)	20. Security Classif.(of this page)	21. No. of Pages	22. Price
Unclassified	Unclassified	62	A04

For sale by the National Technical Information Service, Springfield, Virginia 22161

NASA-Langley, 1987